

Compactifying the Electronic Wavefunction II: Quantum Estimators for Spin-Coupled Generalized Valence Bond Wavefunctions

Bruna Gabrielly^{1, *}

¹*Department of Chemistry, Materials and Chemical Engineering "Giulio Natta",
Politecnico di Milano, Via Bassini 6, 20133 Milano, Italy*

We present a measurement-driven quantum framework for evaluating overlap and Hamiltonian matrix elements in spin-coupled generalized valence bond (SCGVB) wavefunctions. The approach targets a central difficulty of nonorthogonal valence-bond methods: estimating matrix elements between distinct, generally nonorthogonal configuration state functions. Rather than preparing the full wavefunction on quantum hardware, we reformulate the required quantities as vacuum expectation values of Pauli-string operators that can be accessed using shallow, ancilla-free circuits composed of local Clifford rotations and computational-basis measurements. In contrast to Hadamard-test-based matrix-element estimation, this construction avoids ancilla qubits and controlled operations by reducing the problem to local Pauli measurements. This separates the algebraic construction of the SCGVB problem from the measurement task executed on the quantum register and yields a low-depth strategy compatible with near-term architectures. We demonstrate the framework on square and rectangular H₄ using quantum-circuit emulation, where the resulting overlap and Hamiltonian matrices reproduce classical Löwdin-based references with good accuracy across the geometries considered, and where derived Coulson–Chirgwin weights remain chemically consistent. These results support the feasibility of measurement-based quantum assistance for nonorthogonal SCGVB expansions and provide a practical route for incorporating quantum measurements into valence-bond electronic-structure workflows.

I. INTRODUCTION

Generalized valence bond (GVB) theory has evolved into a family of chemically transparent multiconfigurational approaches for describing static correlation in terms of localized bonding patterns. Among its most powerful extensions is the Spin-Coupled Generalized Valence Bond (SCGVB) method [3, 18], which enforces exact total-spin eigenfunctions through the explicit coupling of the spin parts of electron pairs. This construction provides a compact and chemically intuitive framework for describing singlet–triplet mixing, multibond correlation, and bond reorganization processes, while retaining a localized picture of chemical bonding [20]. Related developments, including the Breathing-Orbital Valence Bond (BOVB) method [4] and multiconfigurational SCGVB variants [18], further increase the flexibility of the valence-bond description by allowing orbital relaxation across different valence-bond structures.

Beyond its conceptual appeal, GVB-based theories are also computationally competitive with modern multireference approaches. For simple yet paradigmatic systems such as H₂, H₄, and related molecules, GVB treatments can reproduce near-exact dissociation curves with only a small number of determinants [17, 21], whereas full configuration interaction generally requires an exponentially growing expansion. Within this framework, the resulting generalized eigenvalue problem [Eq. (2)] naturally accommodates orthogonalization procedures such as Löwdin symmetric orthogonalization [2, 22] and enables

quantitative wavefunction analyses, including Chirgwin–Coulson weighting schemes [1, 4].

Despite these advantages, the evaluation of overlap and off-diagonal Hamiltonian matrix elements between nonorthogonal determinants remains a major obstacle, especially in the context of quantum implementations of valence-bond wavefunctions. This difficulty reflects a long-standing challenge already present in classical multiconfigurational electronic-structure theory, where nonorthogonality considerably complicates the algebra of many-electron operators and matrix elements [19]. Recent progress in fermion-to-qubit mappings for nonorthogonal orbital bases has opened new possibilities for quantum simulation in such settings [12]. However, existing quantum subroutines for matrix-element estimation typically rely on ancilla qubits, Hadamard tests, or deep controlled-unitary circuits, all of which are poorly suited to noisy intermediate-scale quantum (NISQ) hardware [26].

In this work, we introduce two ancilla-free quantum estimators tailored to SCGVB determinant spaces. The central idea is to reformulate the required overlap and Hamiltonian matrix elements as vacuum expectation values of Pauli-string operators, so that nonorthogonality, spin coupling, and determinant algebra are treated classically, while the quantum register is used only for shallow measurement tasks. The resulting estimators rely exclusively on local Clifford operations and computational-basis measurements, thereby avoiding ancilla qubits, controlled unitaries, and Hadamard-test-based protocols. In this sense, the present approach should be viewed not as a full quantum realization of the SCGVB ansatz, but rather as a measurement-based quantum backend for nonorthogonal electronic-structure methods such as

* bruna.gabriellyma@gmail.com

SCGVB, formulated within a nonorthogonal Jordan–Wigner framework [12].

From the perspective of computational chemistry, this separation between many-electron algebra and quantum-state manipulation constitutes the main conceptual contribution of the present work. Rather than attempting to prepare the full nonorthogonal wavefunction on quantum hardware, the method directly targets the central bottleneck of SCGVB calculations, namely the reliable evaluation of overlap and Hamiltonian matrix elements between nonorthogonal determinants. Although the H_4 cluster considered here is chemically minimal, within the SCGVB framework, it already generates a nonorthogonal determinant basis and a nontrivial generalized eigenvalue problem, making it a meaningful proof-of-principle benchmark for algorithms designed to handle nonorthogonal determinant algebra. The resulting framework is therefore complementary to classical SCGVB implementations and may be naturally integrated into broader hybrid workflows involving orbital optimization, tensor-network embeddings, or selected configuration-interaction expansions.

The goal of the present work is therefore not to establish a general quantum speedup, but rather to construct a low-depth, ancilla-free estimator framework for nonorthogonal SCGVB matrix-element evaluation.

The present work belongs to a broader research program devoted to the compactification of electronic wavefunctions in strongly correlated systems. In this sense, it is aligned with the direction initiated in our previous study [6], although the two works are methodologically independent and address distinct algorithmic settings.

The remainder of this paper is organized as follows. Section II introduces the theoretical framework of the SCGVB wavefunction and its representation on a nonorthogonal determinant basis. Section III presents the ancilla-free quantum estimators for the evaluation of determinant overlaps and Hamiltonian matrix elements. Section IV describes the computational implementation. Finally, Section V presents the application to the H_4 system and analyzes the accuracy of the overlap and Hamiltonian matrices obtained from the quantum estimators.

II. THEORETICAL FRAMEWORK

A. Spin-Coupled Generalized Valence Bond (SCGVB) Wavefunction

The Generalized Valence Bond (GVB) approach provides a compact and chemically intuitive framework bridging traditional valence bond (VB) and molecular orbital (MO) descriptions of electronic structure. Originally developed by Goddard and co-workers [17], GVB extends the Heitler–London and Pauling VB pictures by allowing the orbitals associated with each electron pair to be nonorthogonal and variationally optimized. This flexibility enables an efficient description of static and

dynamic correlation while maintaining a localized, bond-centered interpretation [4, 18].

In contrast to delocalized Hartree–Fock molecular orbitals, GVB employs localized orbital pairs that describe both covalent and ionic contributions. For a singlet-coupled electron pair, the GVB pair function is

$$\Phi_{\text{pair}} = N [\phi_a(1)\phi_b(2) + \phi_b(1)\phi_a(2)] \chi_{s=0}, \quad (1)$$

where ϕ_a and ϕ_b are generally nonorthogonal spatial orbitals, $\chi_{s=0}$ is the singlet spin function, and N is a normalization constant depending on the orbital overlap $S_{ab} = \langle \phi_a | \phi_b \rangle$. Variation of the pair orbitals in the presence of all other electrons leads to coupled equations analogous to those of Hartree–Fock theory [17, 21, 22]. Because the orbitals are nonorthogonal, the resulting variational problem takes the form of a generalized eigenvalue equation,

$$\mathbf{HC} = \mathbf{SCE}, \quad (2)$$

where \mathbf{H} is the Hamiltonian matrix, \mathbf{S} the overlap matrix, and \mathbf{C} the coefficient matrix describing the linear combination of nonorthogonal configurations $\{\Theta_\mu\}$. This nonorthogonality is crucial for properly describing near-degeneracies, bond breaking, and diradical character in molecular systems [4, 18].

In the spin-coupled generalized valence bond (SCGVB) approach, the many-electron wavefunction for an N -electron system in a spin state characterized by the quantum numbers (S, M) is written as an explicitly spin-adapted linear combination of spin-coupled (SC) structures constructed from generally nonorthogonal spatial orbitals [17, 29–32]. The SCGVB wavefunction can be expressed as

$$\begin{aligned} \Psi_{\text{SCGVB}} &= \mathcal{N} \sum_{k=1}^{f_S^N} c_{S,k} \psi_{S,M;k}^N \\ &= \mathcal{N} \sum_{k=1}^{f_S^N} c_{S,k} \hat{A}(\phi_1 \phi_2 \dots \phi_N \Theta_{S,M;k}^N), \end{aligned} \quad (3)$$

where f_S^N is the number of linearly independent N -electron spin eigenfunctions $\Theta_{S,M;k}^N$ for a given S (see below and Fig. 1), $c_{S,k}$ are spin-coupling coefficients, and \mathcal{N} is a normalization constant ensuring $\langle \Psi_{\text{SCGVB}} | \Psi_{\text{SCGVB}} \rangle = 1$. Each spin-coupled structure $\psi_{S,M;k}^N$ is obtained by applying the antisymmetrizer \hat{A} to a product of N spatial orbitals and one spin eigenfunction. The antisymmetrizer is defined as [21, 22]

$$\hat{A} = \frac{1}{\sqrt{N!}} \sum_{\hat{P} \in S_N} (-1)^p \hat{P}, \quad (4)$$

where the sum runs over all permutations \hat{P} of the N electrons belonging to the symmetric group S_N , and $(-1)^p$ is the parity of the permutation. The set $\{\phi_i\}$ in Eq. (3) denotes the spin-coupled spatial orbitals, which are in

general nonorthogonal, $\langle \phi_i | \phi_j \rangle \neq \delta_{ij}$, and are expanded in a one-electron atomic basis $\{\chi_\mu\}$,

$$\phi_i(\mathbf{r}) = \sum_{\mu=1}^{N_{bf}} C_{\mu i} \chi_\mu(\mathbf{r}), \quad (5)$$

where N_{bf} is the number of basis functions and $C_{\mu i}$ are the orbital expansion coefficients. In practical SCGVB calculations, both the spin-coupling coefficients $\{c_{S,k}\}$ and the orbital coefficients $\{C_{\mu i}\}$ (or, equivalently, the spin-coupled orbitals $\{\phi_i\}$) are determined variationally by energy minimization [3, 29, 30].

It is important to emphasize that the first line of Eq. (3) represents a formally exact expansion of an N -electron eigenfunction in a complete set of spin eigenfunctions $\{\Theta_{S,M;k}^N\}$. The approximation in SCGVB enters through the second line of Eq. (3), where each spin-coupled structure $\psi_{S,M;k}^N$ is represented in terms of a finite set of spin-coupled orbitals $\{\phi_i\}$ and a chosen spin basis $\{\Theta_{S,M;k}^N\}$. In the most general formulation, an additional set of doubly occupied core orbitals may be included. For the hydrogen clusters H_n considered in this work, however, no core orbitals are present, and this complication can be omitted [4, 18].

The branching diagram shown in Fig. 1 provides a convenient visual summary of the spin space entering Eq. (3). Each node at coordinates (N, S) is labelled by

$$f_S^N = \frac{(2S+1)N!}{\left(\frac{N}{2} + S + 1\right)! \left(\frac{N}{2} - S\right)!}, \quad (6)$$

which is the number of linearly independent spin eigenfunctions $\Theta_{S,M;k}^N$ for that electron number and total spin [8, 9, 32]. This number is identical to the range of the index k in Eq. (3). For example, the $N = 4, S = 1$ node is labelled by $f_1^4 = 3$, indicating that the triplet SCGVB wavefunction for four electrons involves three linearly independent spin-coupled structures. Similarly, the $N = 6, S = 0$ node is labelled $f_0^6 = 5$, so the six-electron singlet SCGVB expansion contains five spin-coupled structures. Edges in Fig. 1 connect (N, S) to $(N+1, S \pm \frac{1}{2})$ and represent the allowed couplings when a new spin- $\frac{1}{2}$ electron is added. Thus, the diagram not only encodes the values of f_S^N but also illustrates how the various spin manifolds are generated by successive spin couplings.

a. Spin eigenfunctions and primitive spin functions. Each spin eigenfunction $\Theta_{S,M;k}^N$ can be written as a fixed linear combination of spin primitive functions $\{\theta_i^N\}$, i.e., simple products of one-electron spin functions α and β that are eigenfunctions of \hat{S}_z but not of \hat{S}^2 ,

$$\Theta_{S,M;k}^N = \sum_{i=1}^{N_d} d_{i,k}^S \theta_i^N, \quad (7)$$

where N_d is the number of determinants (or primitive spin functions) with the appropriate spin projection M ,

$$N_d = \binom{N}{N_\alpha} = \binom{N}{N_\beta}, \quad (8)$$

and N_α and N_β are the numbers of α and β spins, respectively. The coefficients $\{d_{i,k}^S\}$ depend on the chosen spin basis (such as Kotani, Serber, or Rumer bases) and can be obtained from standard angular-momentum coupling or group-theoretical arguments [9, 31, 32]. In particular, the Rumer basis provides an irreducible representation of the symmetric group S_N , with coefficients $d_{i,k}^S$ restricted to 0 and ± 1 , which is especially convenient in practical SCGVB implementations. Substituting Eq. (7) into Eq. (3), the SCGVB wavefunction can be recast as

$$\Psi_{\text{SCGVB}} = \mathcal{N} \sum_{i=1}^{N_d} b_{S,i} \hat{A}(\phi_1 \phi_2 \dots \phi_N \theta_i^N), \quad (9)$$

where the coefficients $b_{S,i}$ are given by

$$b_{S,i} = \sum_{k=1}^{f_S^N} c_{S,k} d_{i,k}^S. \quad (10)$$

Since each primitive spin function θ_i^N is a product of N one-electron spin functions, the product $\phi_1 \phi_2 \dots \phi_N \theta_i^N$ is simply a product of N spin orbitals,

$$\phi_1 \phi_2 \dots \phi_N \theta_i^N = \phi_1^i \phi_2^i \dots \phi_N^i, \quad (11)$$

with $\phi_j^i(\mathbf{r}, \sigma) = \phi_j(\mathbf{r}) \omega_j^i(\sigma)$, where ω_j^i is either α or β in the i th primitive function. Application of the antisymmetrizer to a product of spin orbitals generates a Slater determinant, so Eq. (9) becomes

$$\Psi_{\text{SCGVB}} = \mathcal{N} \sum_{i=1}^{N_d} \frac{b_{S,i}}{\sqrt{N!}} |\phi_1^i \phi_2^i \dots \phi_N^i| \equiv \mathcal{N} \sum_{i=1}^{N_d} b_{S,i} \Omega_i, \quad (12)$$

where $\{\Omega_i\}$ denotes a set of non-normalized Slater determinants built from nonorthogonal spin orbitals. Equation (12) shows that the SCGVB wavefunction can be viewed as a particular linear combination of nonorthogonal determinants with spin-coupling information embedded in the coefficients $b_{S,i}$ [3, 29, 30].

b. Normalization and matrix elements. Because the determinants $\{\Omega_i\}$ are constructed from nonorthogonal spin orbitals, they are themselves nonorthogonal and not normalized. Using Löwdin's rules for overlaps and matrix elements between determinants of nonorthogonal spin orbitals [2, 21, 22], the normalization constant can be written as

$$\mathcal{N} = \mathcal{D}^{-1/2}, \quad (13)$$

with

$$\mathcal{D} = \sum_{i,j=1}^{N_d} b_{S,i} b_{S,j} \det[\mathbf{O}_{ij}], \quad (14)$$

where \mathbf{O}_{ij} is the matrix of overlap integrals between the spin orbitals entering determinants Ω_i and Ω_j . Accord-

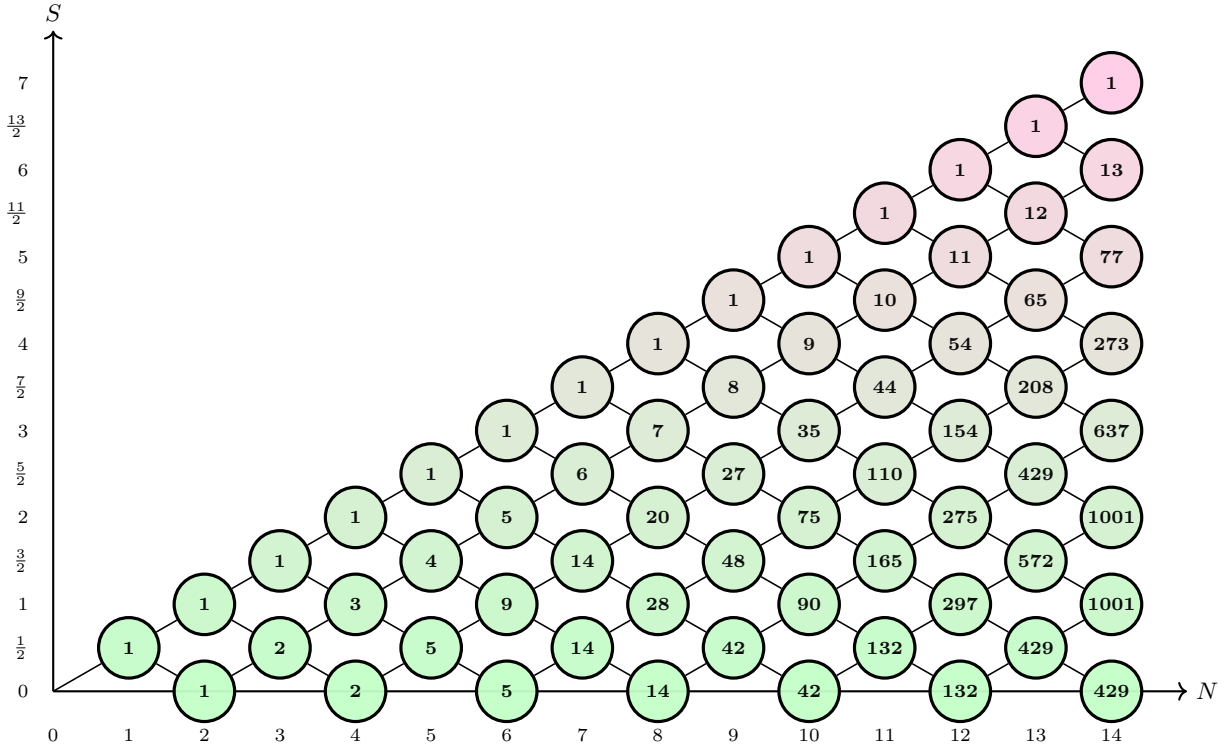


FIG. 1: Branching diagram of spin couplings for $N = 1, \dots, 14$ electrons. Each node at coordinates (N, S) is labeled by $f_S^N = \frac{(2S+1)N!}{(\frac{N}{2}+S+1)!(\frac{N}{2}-S)!}$, which gives the number of linearly independent spin eigenfunctions $\Theta_{S,M;k}^N$ for that electron number and total spin [8, 9, 32]. Edges indicate the allowed couplings when a spin- $\frac{1}{2}$ electron is added, connecting (N, S) to $(N+1, S \pm \frac{1}{2})$. Thus, the integer at each node equals the range of the index k in Eq. (3), and therefore the number of spin-coupled structures entering the SCGVB expansion for that (N, S) . The color gradient (from light pink to light green) indicates increasing total spin S . Adapted from R. McWeeny [8] and R. Pauncz [9].

ingly, Eq. (12) may also be written as

$$\Psi_{\text{SCGVB}} = \mathcal{D}^{-1/2} \sum_{i=1}^{N_d} \frac{b_{S,i}}{\sqrt{N!}} |\phi_1^i \phi_2^i \dots \phi_N^i|, \quad (15)$$

$$= \mathcal{D}^{-1/2} \sum_{i=1}^{N_d} b_{S,i} \Omega_i. \quad (16)$$

The SCGVB wavefunction is determined variationally by minimizing the energy functional

$$E[\Psi_{\text{SCGVB}}] = \frac{\langle \Psi_{\text{SCGVB}} | \hat{H} | \Psi_{\text{SCGVB}} \rangle}{\langle \Psi_{\text{SCGVB}} | \Psi_{\text{SCGVB}} \rangle}, \quad (17)$$

is minimized with respect to both orbital and spin-coupling coefficients. Evaluation of the required overlaps and Hamiltonian matrix elements constitutes the dominant computational bottleneck of SCGVB and related VB methods [29, 33], motivating alternative strategies such as quantum computing.

Löwdin Symmetric Orthogonalization of the VB Basis

To simplify the solution of Eq. (2), it is convenient to transform the nonorthogonal basis $\{\Theta_\mu\}$ into an orthonormal one, $\{\Theta'_\mu\}$, by means of a symmetric orthogonalization transformation [2, 16]. This procedure, introduced by Löwdin in 1950, guarantees that the orthogonalization preserves the symmetry and near-local character of the original VB structures, while minimizing the distortion of the orbital subspace [2, 16, 21, 22]. The transformation is defined as

$$\Theta'_\mu = \sum_\nu \Theta_\nu X_{\nu\mu}, \quad (18)$$

or, in matrix notation,

$$\Theta' = \Theta \mathbf{X}, \quad (19)$$

where the transformation matrix \mathbf{X} satisfies the orthonormality condition

$$\mathbf{X}^\dagger \mathbf{S} \mathbf{X} = \mathbf{I}. \quad (20)$$

The unique Hermitian matrix fulfilling this requirement is the symmetric Löwdin transformation,

$$\mathbf{X} = \mathbf{S}^{-1/2}. \quad (21)$$

Because $\mathbf{S}^{-1/2}$ is Hermitian, this transformation ensures that the orthogonalized basis retains the symmetry properties of the original VB structures [2, 22]. Such orthogonalization is routinely employed in many-body electronic structure theory, including configuration interaction, coupled cluster, and tensor network formulations [11, 21, 22].

Transformation of the Hamiltonian and Coefficients

Upon orthogonalization, the total wavefunction can be equivalently written as

$$\Psi_i = \Theta' \mathbf{C}' = \Theta \mathbf{X} \mathbf{C}', \quad (22)$$

which implies that the coefficients in the nonorthogonal and orthogonal representations are related by

$$\mathbf{C} = \mathbf{X} \mathbf{C}' = \mathbf{S}^{-1/2} \mathbf{C}'. \quad (23)$$

Substituting this into Eq. (2) yields

$$\mathbf{H} \mathbf{X} \mathbf{C}' = \mathbf{S} \mathbf{X} \mathbf{C}' \mathbf{E}. \quad (24)$$

Multiplying both sides by \mathbf{X}^\dagger and using Eq. (20), we obtain the orthogonalized secular equation

$$\mathbf{H}' \mathbf{C}' = \mathbf{C}' \mathbf{E}, \quad (25)$$

where the transformed Hamiltonian is defined as

$$\mathbf{H}' = \mathbf{X}^\dagger \mathbf{H} \mathbf{X} = \mathbf{S}^{-1/2} \mathbf{H} \mathbf{S}^{-1/2}. \quad (26)$$

Diagonalization of \mathbf{H}' yields the eigenvalues \mathbf{E} and the orthogonalized coefficients \mathbf{C}' , from which the original coefficients \mathbf{C} can be recovered via Eq. (23). This transformation formalism forms the mathematical foundation of spin-coupled VB theory and its modern extensions to multireference and tensor-based frameworks [3, 4, 18, 22].

Once the orthogonalized coefficients \mathbf{C}' and the overlap matrix \mathbf{S} are available, the quantitative analysis of individual VB structure contributions to the total wavefunction can be performed using the *Chirgwin–Coulson weights* [1, 3–5, 7]. These weights provide a rigorous way to measure the relative importance of each spin-coupled structure in the final SCGVB state, offering both interpretability and a direct connection to chemical bonding concepts. In the following section, we present a detailed derivation and discussion of these weights, along with their numerical evaluation and interpretational limitations.

Chirgwin–Coulson Weights

Chirgwin–Coulson weights are introduced here because they provide a chemically interpretable diagnostic that will be used in the analysis of the quantum results later.

Once the generalized eigenvalue problem (Eq. 2) is solved, the coefficients \mathbf{C} obtained in the nonorthogonal valence-bond (VB) basis $\{\Theta_\mu\}$ can be used to analyze the relative importance of individual VB structures. A standard quantitative measure for this purpose is provided by the *Chirgwin–Coulson (CC) weights*, originally introduced by Chirgwin and Coulson [1]. For a nonorthogonal expansion

$$|\Psi\rangle = \sum_i C_i |\Phi_i\rangle, \quad (27)$$

with overlaps $S_{ij} = \langle \Phi_i | \Phi_j \rangle$, the CC weight associated with structure i is defined as

$$W_i = \sum_j C_i C_j S_{ij}. \quad (28)$$

In an orthonormal basis ($S_{ij} = \delta_{ij}$), this expression reduces to the familiar form $W_i = |C_i|^2$.

In the general nonorthogonal case, the overlap terms introduce interference contributions, so that W_i depends both on coefficient magnitudes and on mutual overlaps between structures. As a result, CC weights are not strictly probabilistic quantities, but rather relative indicators of structural importance in the total wavefunction [3–5, 7]. Two well-known consequences of nonorthogonality follow. First, individual CC weights are not constrained to the interval $[0, 1]$ and may even become negative for strongly overlapping structures [3, 5]. Second, the total sum $\sum_i W_i$ is not guaranteed to be exactly unity, particularly in the presence of near-linear dependencies in the VB basis [4, 7].

In chemically well-behaved cases, however, CC weights typically remain positive and sum to approximately one, allowing a clear distinction between dominant and secondary VB structures [4]. When deviations from this behavior occur, it is customary either to report them explicitly or to complement the analysis with alternative weighting schemes. Two commonly used modified definitions are the Löwdin weights,

$$W_i^{(L)} = \sum_{j,k} S_{ij}^{1/2} C_j S_{ik}^{1/2} C_k, \quad (29)$$

obtained after symmetric orthogonalization of the VB basis, and the inverse weights,

$$W_i^{(inv)} = \frac{C_i^2 / (S^{-1})_{ii}}{\sum_j C_j^2 / (S^{-1})_{jj}}, \quad (30)$$

which suppress the contribution of strongly overlapping structures and enforce $0 \leq W_i^{(inv)} \leq 1$ [2, 4]. Although

these definitions differ numerically, they generally preserve the qualitative ordering of structure importance and serve as consistency checks for CC analyses.

In this work, CC weights are computed directly from Eq. (28) using the coefficients and overlap matrix obtained from Eq. (2). For the two-structure case relevant to the $\text{H}_4 \rightleftharpoons 2\text{H}_2$ system,

$$W_1 = |C_1|^2 + C_1 C_2 S_{12}, \quad (31)$$

$$W_2 = |C_2|^2 + C_1 C_2 S_{21}. \quad (32)$$

The practical procedure consists of constructing the overlap matrix, solving the generalized eigenvalue problem, evaluating the CC weights, and verifying their physical consistency. Dominant structures typically exhibit $W_i \gtrsim 0.5$, while smaller values indicate secondary contributions. When CC weights become negative or exceed unity, this signals strong overlap effects, and the alternative definitions in Eqs. (29)–(30) should be preferred for quantitative interpretation.

Throughout this work we restrict attention to ground states within a fixed total-spin sector. Extensions to excited states would require substantially larger spin-coupling spaces and are beyond the scope of the present near-term quantum algorithm.

B. Nonorthogonal Jordan–Wigner mapping

To represent the SCGVB Hamiltonian and determinant operators on a qubit register, we adopt the nonorthogonal Jordan–Wigner (NOJW) fermion–qubit mapping introduced in Ref. [12]. The SCGVB ansatz introduced above is expressed in a generally nonorthogonal spin-orbital basis and therefore leads naturally to a nonorthogonal second-quantized Hamiltonian.

Nonorthogonal second quantization and auxiliary bases

Let $\{\varphi_p(x)\}_{p=1}^M$ be a set of nonorthogonal spin orbitals with overlap matrix

$$S_{pq} = \int dx \varphi_p^*(x) \varphi_q(x), \quad \mathbf{S} = [S_{pq}], \quad (33)$$

where x collects spatial and spin coordinates. Creation operators $\{\hat{a}_p^\dagger\}$ and their adjoints $\{\hat{a}_p\}$ obey the generalized anticommutation relations

$$\{\hat{a}_p, \hat{a}_q\}_+ = 0, \quad (34)$$

$$\{\hat{a}_p^\dagger, \hat{a}_q^\dagger\}_+ = 0, \quad (35)$$

$$\{\hat{a}_p, \hat{a}_q^\dagger\}_+ = S_{pq}, \quad (36)$$

which reduce to the canonical CAR when $\mathbf{S} = \mathbf{I}$. The electronic Hamiltonian in this basis reads

$$\hat{H} = \sum_{p,q=1}^M h_{pq} \hat{a}_p^\dagger \hat{a}_q + \frac{1}{2} \sum_{p,q,r,s=1}^M g_{pqrs} \hat{a}_p^\dagger \hat{a}_q^\dagger \hat{a}_s \hat{a}_r, \quad (37)$$

with one- and two-electron integrals evaluated in the nonorthogonal orbitals, so that in general $h_{pq} \neq h_{qp}$ and $g_{pqrs} \neq g_{rspq}$.

For later use, we introduce two auxiliary orbital sets. First, a symmetrically orthogonalized basis is obtained via Löwdin orthogonalization,

$$\tilde{\varphi}_p(x) = \sum_{q=1}^M \varphi_q(x) [S^{-1/2}]_{qp}, \quad \langle \tilde{\varphi}_p | \tilde{\varphi}_q \rangle = \delta_{pq}, \quad (38)$$

with associated operators $\{\hat{a}_p^\dagger, \hat{a}_p\}$ satisfying the canonical CAR. The two operator sets are related by

$$\hat{a}_p^\dagger = \sum_{q=1}^M \hat{a}_q^\dagger [S^{-1/2}]_{qp}, \quad (39)$$

$$\hat{a}_p^\dagger = \sum_{q=1}^M \hat{a}_q^\dagger [S^{1/2}]_{qp}, \quad (40)$$

and similarly for their adjoints. Thus \hat{a}_p is the Hermitian adjoint of \hat{a}_p^\dagger but not a canonical annihilation operator when $\mathbf{S} \neq \mathbf{I}$.

Second, we define the biorthogonal partner orbitals

$$\varphi^p(x) = \sum_{q=1}^M \varphi_q(x) [S^{-1}]_{qp}, \quad \langle \varphi^p | \varphi_q \rangle = \delta_{pq}^p, \quad (41)$$

with corresponding annihilation operators $\{\hat{b}_p\}$ satisfying

$$\{\hat{b}_p, \hat{a}_q^\dagger\}_+ = \delta_{pq}, \quad (42)$$

and

$$\hat{b}_p = \sum_{q=1}^M [S^{-1}]_{pq} \hat{a}_q. \quad (43)$$

In the biorthogonal operator set $\{\hat{a}_p^\dagger, \hat{b}_p\}$ the Hamiltonian can be rewritten as

$$\hat{H} = \sum_{p,q=1}^M \tilde{h}_{pq} \hat{a}_p^\dagger \hat{b}_q + \frac{1}{2} \sum_{p,q,r,s=1}^M \tilde{g}_{pqrs} \hat{a}_p^\dagger \hat{a}_q^\dagger \hat{b}_s \hat{b}_r, \quad (44)$$

with effective integrals \tilde{h}_{pq} and \tilde{g}_{pqrs} obtained by contraction with \mathbf{S}^{-1} (see, e.g., Refs. [2, 8]). This representation will be particularly convenient for encoding \hat{H} on qubits.

Jordan–Wigner encoding for nonorthogonal orbitals

We now outline the fermion–qubit mapping suitable for the operator sets $\{\hat{a}_p^\dagger, \hat{a}_p\}$ and $\{\hat{b}_p\}$, following the nonorthogonal Jordan–Wigner construction of Ref. [12]. Each spin orbital is associated with a qubit, and we use the usual ON basis $\{|k_1, \dots, k_M\rangle\}$, where $k_p \in \{0, 1\}$ denotes the occupation of the orbital p .

On an orthonormal basis, the standard Jordan-Wigner encoding [21, 22] maps the creation operator to

$$\hat{a}_p^\dagger \longleftrightarrow Z_1 \otimes \cdots \otimes Z_{p-1} \otimes \frac{X_p - iY_p}{2} \otimes I_{p+1} \otimes \cdots \otimes I_M, \quad (45)$$

with the annihilation operator obtained by Hermitian conjugation. Here X_p , Y_p , and Z_p are Pauli matrices acting on qubit p , and I_p is the identity.

Because $\{\hat{a}_p^\dagger, \hat{a}_p\}$ obey the canonical CAR, Eq. (45) defines a valid fermion-qubit mapping. Using Eqs. (39)–(40), any nonorthogonal operator can be written as a linear combination of orthonormal operators and thus as a linear combination of JW strings. In particular, by absorbing the orbital transformation into the definition of the φ_p and of the integrals, the nonorthogonal creation operators inherit the same JW string structure as in the orthogonal case,

$$\hat{a}_p^\dagger \longleftrightarrow Z_1 \otimes \cdots \otimes Z_{p-1} \otimes \frac{X_p - iY_p}{2} \otimes I_{p+1} \otimes \cdots \otimes I_M. \quad (46)$$

The adjoint operators \hat{a}_p require a different treatment. Using Eq. (36), one can show that applying \hat{a}_p to an ON state $|k_1, \dots, k_M\rangle$ yields a linear combination of states in which one of the occupied orbitals q is emptied, with coefficients proportional to S_{pq} . This motivates the following JW-like encoding:

$$\hat{a}_p \longleftrightarrow \sum_{q=1}^M S_{pq} \left[Z_1 \otimes \cdots \otimes Z_{q-1} \otimes \frac{X_q + iY_q}{2} \otimes I_{q+1} \otimes \cdots \otimes I_M \right], \quad (47)$$

that is, a weighted sum of standard JW annihilation strings, with weights given by the overlap matrix elements S_{pq} . One can verify explicitly that the images of \hat{a}_p^\dagger and \hat{a}_q under Eqs. (46)–(47) satisfy the generalized anticommutation relations (36) when acting on the qubit basis.

The mapping in Eq. (47) provides a direct encoding of wavefunctions built from nonorthogonal determinants, such as the SCGVB determinants introduced earlier, onto a quantum register. However, because each \hat{a}_p is represented as a sum of Pauli strings, the number of distinct strings appearing in the qubit Hamiltonian of Eq. (37) scales in the worst case as $\mathcal{O}(M^3)$ for the one-electron term and $\mathcal{O}(M^6)$ for the two-electron term, which is significantly less favorable than the $\mathcal{O}(M^2)$ and $\mathcal{O}(M^4)$ scalings of the conventional JW mapping in an orthonormal basis.

While the nonorthogonal Jordan-Wigner mapping defines how operators are represented on qubits, it does not address the dominant NISQ bottleneck: the evaluation of overlaps and off-diagonal Hamiltonian matrix elements between nonorthogonal determinants. In practice, this task is commonly addressed via Hadamard-test-based schemes, which require ancilla qubits, controlled operations, and deep circuits. In the following, we introduce quantum estimators that resolve this bottleneck using only shallow, ancilla-free, and control-free circuits.

III. SCGVB-INSPIRED QUANTUM ALGORITHMS

The nonorthogonal generalized valence bond (SCGVB) ansatz requires the evaluation of two classes of quantities: (i) overlaps between nonorthogonal Slater determinants $\langle \psi_j | \psi_i \rangle$, and (ii) Hamiltonian matrix elements $H_{ij} = \langle \psi_j | \hat{H} | \psi_i \rangle$. On a quantum device, overlaps and expectation values are commonly evaluated using ancilla-based Hadamard tests or modified Hadamard-test variants relying on controlled-unitary operations [23–26], which introduce additional qubit and coherence overhead.

Although powerful, these approaches require controlled unitaries, entangling gates, and circuits whose depth scales with the Pauli decomposition of the operators, making them poorly suited for NISQ hardware. Here we introduce a pair of NISQ-compatible quantum estimators that compute both classes of quantities without using variational parameters, controlled operations, or ancilla qubits.

We define two primitives:

- **SCGVB Determinant-Overlap Estimator (DOE)**: a direct probability-estimation scheme for evaluating $\langle \psi_j | \psi_i \rangle$ from the probability of the all-zero outcome after applying the Pauli strings associated with the SCGVB determinants.
- **SCGVB Pauli-Grouped Hamiltonian Estimator (PGHE)**: a measurement-based expectation-value estimator for $\langle \psi_j | \hat{H} | \psi_i \rangle$, based on qubit-wise commuting (QWC) grouping and local basis rotations.

In contrast to ancilla-based approaches, the SCGVB-NOQA framework introduced here replaces all controlled operations by purely local, single-qubit Clifford circuits. Both estimators are ancilla-free, non-variational, and contain no entangling gates. All measurements reduce to sampling in rotated computational bases, and all Pauli groups are evaluated via shallow, constant-depth circuits. To the best of our knowledge, this constitutes the first explicitly formulated fully local, ancilla-free quantum evaluation scheme tailored to SCGVB determinant spaces.

Resource comparison with ancilla-based estimators. Before detailing the estimators, we briefly contrast their resource requirements with those of ancilla-based approaches. Ancilla-based methods for evaluating overlaps or transition amplitudes, such as the Hadamard test, require an additional control qubit on top of the system register, resulting in $n + 1$ qubits for an n -qubit system. Modified Hadamard-test schemes used to estimate general matrix elements of the form $\langle \psi | \hat{O} | \phi \rangle$ typically require two system registers together with an ancilla qubit, leading to $2n + 1$ qubits.

In contrast, the estimators introduced in this work act directly on a single system register and require only n qubits. Moreover, the proposed circuits avoid controlled unitaries entirely and consist solely of local single-qubit

Clifford operations followed by computational-basis measurements, resulting in constant-depth circuit implementations.

This section now presents the complete formulation of the two estimators, including their circuit constructions, measurement rules, and asymptotic scaling.

A. SCGVB Determinant–Overlap Estimator (DOE)

We evaluate the overlap matrix elements of the form

$$\langle \psi_j | \psi_i \rangle, \quad |\psi_i\rangle = \hat{f}_i |\text{vac}\rangle, \quad \langle \psi_j| = \langle \text{vac}| \hat{w}_j, \quad (48)$$

where $|\text{vac}\rangle = |0\rangle^{\otimes n}$ denotes the computational-basis vacuum. Each determinant operator \hat{f}_i or \hat{w}_j corresponds to a product of fermionic creation and annihilation operators, respectively. After applying the nonorthogonal Jordan–Wigner mapping into \hat{w}_j and the standard JW into \hat{f}_i , each operator becomes a linear combination of n -qubit Pauli strings:

$$\hat{f}_i = \sum_a c_{i,a}^{(f)} Q_{i,a}, \quad \hat{w}_j = \sum_b c_{j,b}^{(w)} P_{j,b}, \quad (49)$$

where $Q_{i,a}$ and $P_{j,b}$ are tensor products of $\{X, Y, Z, I\}$ operators. These Pauli terms are stored externally and loaded directly by the quantum routine.

a. Circuit construction. Expanding both operators yields

$$\langle \psi_j | \psi_i \rangle = \sum_{a,b} c_{i,a}^{(f)} c_{j,b}^{(w)} \langle 0^n | P_{j,b} Q_{i,a} | 0^n \rangle. \quad (50)$$

Our algorithm evaluates each Pauli-pair contribution $\langle 0^n | P_{j,b} Q_{i,a} | 0^n \rangle$ using the shallow Clifford circuit shown in Fig. 2:

1. initialize the register in $|0\rangle^{\otimes n}$;
2. apply all non-identity Pauli gates in $Q_{i,a}$;
3. apply all non-identity Pauli gates in $P_{j,b}$;
4. measure all qubits in the computational basis.

Because Pauli operators act locally and require no entangling gates, the circuit depth is $\mathcal{O}(1)$ and depends only on the number of non-identity Pauli factors in $P_{j,b} Q_{i,a}$.

b. Measurement rule. The measurement samples from the distribution generated by $P_{j,b} Q_{i,a} | 0^n \rangle$. Because a Pauli string maps the vacuum to a single computational-basis state (up to a phase), the probability of obtaining the all-zero outcome,

$$p_{ab}^{(ij)} = \Pr(0^n | P_{j,b} Q_{i,a} | 0^n), \quad (51)$$

directly encodes the magnitude of the amplitude $\langle 0^n | P_{j,b} Q_{i,a} | 0^n \rangle$. The full overlap is reconstructed via linearity:

$$\tilde{O}_{ij} = \sum_{a,b} c_{i,a}^{(f)} c_{j,b}^{(w)} p_{ab}^{(ij)}. \quad (52)$$

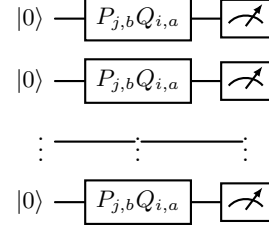


FIG. 2: Quantum circuit used to evaluate a single Pauli-pair contribution $\langle 0^n | P_{j,b} Q_{i,a} | 0^n \rangle$. Since each Pauli string is a tensor product of single-qubit Clifford gates. The circuit consists only of local operations followed by computational basis measurement.

No ancilla qubits, controlled unitaries, or mid-circuit measurements are required.

c. Computational scaling. Let $n_{\text{Pauli}}^{(f)}$ and $n_{\text{Pauli}}^{(w)}$ denote the number of Pauli strings in \hat{f}_i and \hat{w}_j , respectively. Each pair $(Q_{i,a}, P_{j,b})$ requires one shallow circuit execution. Thus a single overlap evaluation scales as

$$\mathcal{O}\left(n_{\text{Pauli}}^{(f)} n_{\text{Pauli}}^{(w)}\right), \quad (53)$$

and computing all overlaps between N_f “bra” and N_w “ket” states scales as

$$\mathcal{O}\left(N_f N_w n_{\text{Pauli}}^{(f)} n_{\text{Pauli}}^{(w)}\right). \quad (54)$$

The procedure is embarrassingly parallel over (i, j) and over Pauli-pair indices (a, b) . The corresponding pseudocode is given in Algorithm III A 0 c.

Algorithm 1. Determinant–Overlap Estimator (DOE) for evaluating $\langle \psi_j | \psi_i \rangle$.

Require: Pauli expansions $\hat{f}_i = \sum_a c_{i,a}^{(f)} Q_{i,a}$, $\hat{w}_j = \sum_b c_{j,b}^{(w)} P_{j,b}$; number of shots S .

Ensure: Estimate \tilde{O}_{ij}

- 1: $\tilde{O}_{ij} \leftarrow 0$
- 2: **for** each Pauli string $Q_{i,a}$ in \hat{f}_i **do**
- 3: **for** each Pauli string $P_{j,b}$ in \hat{w}_j **do**
- 4: prepare $|0^n\rangle$
- 5: apply Pauli gates corresponding to $Q_{i,a}$
- 6: apply Pauli gates corresponding to $P_{j,b}$
- 7: measure all qubits in the computational basis
- 8: S times $p_{ab}^{(ij)} \leftarrow \Pr(0^n)$ from measurement statistics
- 9: $\tilde{O}_{ij} \leftarrow \tilde{O}_{ij} + c_{i,a}^{(f)} c_{j,b}^{(w)} p_{ab}^{(ij)}$
- 10: **end for**
- 11: **end for**
- 12: **return** \tilde{O}_{ij}

B. SCGVB Pauli-Grouped Hamiltonian Estimator (PGHE)

While determinant overlaps can be evaluated directly using Pauli applications on the vacuum, the evaluation

of Hamiltonian matrix elements requires estimation of Pauli expectation values. This leads to a different circuit structure, detailed below. We evaluate matrix elements of the form

$$H_{ij} \equiv \langle \phi_0 | w_i \hat{H} f_j | \phi_0 \rangle, \quad (55)$$

where f_j and w_i are the fermionic excitation and de-excitation operators defining the SCGVB determinant basis, mapped to qubits through the nonorthogonal Jordan–Wigner transformation. Each operator is expanded as a sparse linear combination of Pauli strings,

$$f_j = \sum_{\alpha} c_{\alpha}^{(f_j)} P_{\alpha}, \quad w_i = \sum_{\beta} c_{\beta}^{(w_i)} P_{\beta}, \quad \hat{H} = \sum_{\gamma} h_{\gamma} P_{\gamma}. \quad (56)$$

The operator whose expectation value must be measured is

$$\hat{O}_{ij} = w_i \hat{H} f_j = \sum_k d_k^{(ij)} P_k, \quad (57)$$

with coefficients $d_k^{(ij)}$ obtained by symbolic multiplication of Pauli terms. The reference state used throughout is the computational-basis vacuum, $|\phi_0\rangle = |0 \dots 0\rangle$.

a. Measurement strategy. Each Pauli operator P_k appearing in Eq. (57) is measured using a standard basis-rotation protocol. For a single-qubit Pauli,

$$X \rightarrow HZH, \quad (58)$$

$$Y \rightarrow S^{\dagger} HZHS, \quad (59)$$

$$Z \rightarrow Z, \quad I \rightarrow I, \quad (60)$$

so that the composite rotation U_k diagonalizes the full Pauli string. After applying U_k , all qubits are measured in the computational (Z) basis. For a measurement outcome $b \in \{0, 1\}^n$, the eigenvalue is reconstructed via

$$\lambda_k(b) = (-1)^{\sum_{q \in \text{supp}(P_k)} b_q}.$$

b. Qubit-wise commuting (QWC) grouping. To reduce measurement overhead, the Pauli strings $\{P_k\}$ are partitioned into qubit-wise commuting groups,

$$\{P_k\} = G_1 \cup G_2 \cup \dots \cup G_M, \quad [P_k, P_{k'}] = 0 \quad \forall P_k, P_{k'} \in G_{\ell}.$$

All operators in the same group share the same diagonalizing rotation. Thus each G_{ℓ} requires only one circuit execution. This measurement procedure is summarized in the Pauli-Grouped Hamiltonian Estimator (PGHE), shown in **Algorithm III B 0 c**, and the corresponding quantum circuit structure is shown in **Figure 3**.

c. Reconstruction of the matrix element. From repeated measurements (shots) of each QWC group G_{ℓ} , we compute $\langle P_k \rangle_0$ for all $P_k \in G_{\ell}$ and reconstruct

$$H_{ij} = \langle \phi_0 | \hat{O}_{ij} | \phi_0 \rangle = \sum_k d_k^{(ij)} \langle P_k \rangle_0. \quad (61)$$

This process is repeated for all $i, j \in \{1, \dots, N_{\text{det}}\}$, where $N_{\text{det}} = 6$ in the SCGVB space used here.

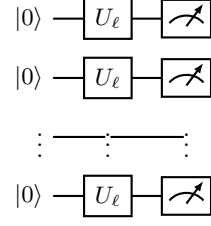


FIG. 3: Quantum circuit used to measure all Pauli operators $P_k \in G_{\ell}$ belonging to a qubit-wise commuting group. A single local basis rotation U_{ℓ} simultaneously diagonalizes every operator in G_{ℓ} , after which all qubits are measured in the computational basis. The resulting bitstring statistics are reused to obtain $\langle P_k \rangle_0$ for all $P_k \in G_{\ell}$, which are then assembled to recover H_{ij} .

Algorithm 2. Pauli-Grouped Hamiltonian Estimator (PGHE) for evaluating $H_{ij} = \langle \phi_0 | w_i H f_j | \phi_0 \rangle$.

Require: Pauli expansion $\hat{O}_{ij} = \sum_k d_k^{(ij)} P_k$, QWC grouping routine $\text{GroupQWC}(\{P_k\})$, number of shots S .

Ensure: Estimate \tilde{H}_{ij}

- 1: $\tilde{H}_{ij} \leftarrow 0$
- 2: $\{G_1, \dots, G_M\} \leftarrow \text{GroupQWC}(\{P_k\})$
- 3: **for** each group G_{ℓ} **do**
- 4: choose representative Pauli $P_{\text{rep}} \in G_{\ell}$
- 5: prepare $|\phi_0\rangle = |0^n\rangle$
- 6: apply basis-rotation U_{ℓ} diagonalizing every $P_k \in G_{\ell}$
- 7: measure all qubits in the Z basis S times
- 8: **for** each $P_k \in G_{\ell}$ **do**
- 9: compute eigenvalues $\lambda_k(b)$ from bitstrings b
- 10: $\langle P_k \rangle_0 = \frac{1}{S} \sum_b \lambda_k(b) p(b)$
- 11: $\tilde{H}_{ij} \leftarrow \tilde{H}_{ij} + d_k^{(ij)} \langle P_k \rangle_0$
- 12: **end for**
- 13: **end for**
- 14: **return** \tilde{H}_{ij}

d. Comparison with the overlap estimator. The Hamiltonian estimator described above is structurally similar to the overlap-evaluation circuit of Sec. III A, but with two key differences. (i) The overlap $\langle \psi_j | \psi_i \rangle$ requires applying the Pauli operators associated with the determinant creation/annihilation operators (f_i, w_j) directly to the vacuum and measuring the probability of the all-zero outcome. No basis rotations or grouping are needed, and the resulting circuits consist only of single-qubit Clifford gates with constant depth. (ii) The Hamiltonian estimator, instead, measures expectation values of the Pauli operators appearing in $\hat{O}_{ij} = w_i H f_j$. Because these Pauli strings must be measured in their eigenbases, a basis rotation is required for each qubit-wise commuting (QWC) group. Consequently, Hamiltonian estimation involves more circuit executions, but each circuit remains extremely shallow (a single layer of local rotations followed by measurement). Both estimators are ancilla-free, deterministic, and use only single-qubit gates, mak-

ing them compatible with NISQ or early fault-tolerant hardware.

e. Computational scaling. Let $n_P^{(f)}$, $n_P^{(w)}$, and $n_P^{(H)}$ denote the number of Pauli terms in the expansions of f_j , w_i , and \hat{H} , respectively. Forming the operator $\hat{O}_{ij} = w_i H f_j$ involves symbolic multiplication of Pauli strings, yielding

$$n_P^{(O)}(i, j) \sim \mathcal{O}\left(n_P^{(f)} n_P^{(w)} n_P^{(H)}\right),$$

after term-combination and cancellation. These $n_P^{(O)}$ Pauli operators must be partitioned into qubit-wise commuting groups $\{G_\ell\}_{\ell=1}^{M_{ij}}$. Since each group requires one circuit execution, the number of quantum circuits for element (i, j) is

$$M_{ij} \leq n_P^{(O)}(i, j),$$

with equality in the worst case (no commuting structure) and typically $M_{ij} \ll n_P^{(O)}(i, j)$ for electronic-structure Hamiltonians.

Each circuit has constant depth and uses only n single-qubit gates, so the total quantum cost per matrix element is

$$\mathcal{Q}_{ij} = \mathcal{O}(M_{ij} \cdot S),$$

where S is the number of measurement shots. For a determinant space of size N_{det} , the full Hamiltonian requires

$$\mathcal{O}(N_{\text{det}}^2 M_{\text{avg}} S)$$

quantum operations, where M_{avg} is the average number of QWC groups per matrix element. Because all (i, j) evaluations and all QWC groups are independent, the entire procedure parallelizes naturally over GPUs, CPUs, or distributed quantum backends.

Although the two-electron Hamiltonian typically contains a significantly larger number of Pauli terms than the one-electron part, the number of required quantum circuits is governed by the number of qubit-wise commuting (QWC) groups rather than by the total number of Pauli strings. In practice, many two-body Pauli terms share identical local support patterns and commute qubit-wise, allowing them to be measured within the same circuit. As a result, the effective number of circuits required for the two-body contribution can be comparable to that of the one-body term, despite the much larger Pauli expansion. For larger systems, related measurement ideas inspired by local quantum overlapping tomography [10] may also prove useful.

It is worth noting that, although the Hadamard test and modified Hadamard-test schemes [23–26] can in principle be used to evaluate the same matrix elements, such techniques require ancilla qubits, controlled operations, and deeper circuits. The approach introduced here avoids

all controlled unitaries, uses only single-qubit Clifford rotations, and therefore provides a lower-overhead NISQ-compatible alternative for the SCGVB nonorthogonal framework.

At first sight, the circuits used in the present estimators consist only of single-qubit Clifford operations acting on computational-basis states, and therefore fall within the class of circuits efficiently simulable according to the Gottesman–Knill theorem. This observation is correct, but does not address the computational bottleneck relevant for nonorthogonal electronic-structure methods.

In the SCGVB framework, the difficulty lies not in simulating individual circuits but in evaluating extremely large numbers of Pauli-string expectation values arising from the combinatorial expansion of nonorthogonal fermionic operators under the Jordan–Wigner mapping. Each matrix element of the Hamiltonian requires the aggregation of many such contributions.

The role of the quantum processor in the present approach is therefore not to generate non-classical states but to serve as a hardware measurement engine capable of sampling Pauli operators directly on qubit registers. By eliminating ancilla qubits and controlled operations, the proposed estimators minimize circuit depth and allow these measurements to be performed using extremely shallow circuits compatible with near-term hardware.

Importantly, the present estimators are designed as modular building blocks. When embedded in broader quantum pipelines involving nontrivial state preparation—such as quantum orbital optimization, tensor-network embeddings, or hybrid VB–VQE schemes—the measurement advantage persists while the overall computation becomes genuinely quantum.

IV. DETAILS OF IMPLEMENTATION

Molecular geometries, atomic-orbital bases, and one- and two-electron integrals were generated using PySCF [27]. The resulting nonorthogonal second-quantized Hamiltonian was constructed and mapped to qubit operators within Qiskit [28]. All quantum estimators described in Sec. III were implemented directly at the Pauli-string level, without the use of ancilla qubits or controlled operations. For completeness and reproducibility, a step-by-step pseudocode description of the Qiskit implementation of the nonorthogonal Jordan–Wigner mapping [12] is provided in Appendix A.

A. SCGVB wavefunction of H_4 in a Singlet State

To make the preceding formalism more concrete, consider the H_4 cluster in its singlet ground state ($S = 0$, $M = 0$). For $N = 4$ electrons and $S = 0$, there are $f_0^4 = 2$ linearly independent spin eigenfunctions, corresponding to two distinct spin-coupling patterns (“pairings”) of the four electrons [29, 31]. The SCGVB wavefunction can

therefore be written as

$$\begin{aligned}\Psi_{\text{SCGVB}} &= \mathcal{N} \left[c_1 \psi_{0,0;1}^4 + c_2 \psi_{0,0;2}^4 \right] \\ &= \mathcal{N} \left[c_1 \hat{A} \left(\phi_1 \phi_2 \phi_3 \phi_4 \Theta_{0,0;1}^4 \right) + \right. \\ &\quad \left. c_2 \hat{A} \left(\phi_1 \phi_2 \phi_3 \phi_4 \Theta_{0,0;2}^4 \right) \right], \quad (62)\end{aligned}$$

where c_1 and c_2 are spin-coupling coefficients that will be determined by minimizing Eq. (17), and ϕ_1, \dots, ϕ_4 are the (generally nonorthogonal) spin-coupled molecular orbitals. Adopting the Rumer basis, the two spin eigenfunctions for $S = 0$ can be written as products of singlet pairs: in one case the pairs are (1,2) and (3,4), in the other (1,4) and (2,3).

Explicitly,

$$\Theta_{0,0;1}^4 = \frac{1}{\sqrt{2}} \left(\alpha_1 \beta_2 - \beta_1 \alpha_2 \right) \frac{1}{\sqrt{2}} \left(\alpha_3 \beta_4 - \beta_3 \alpha_4 \right), \quad (63)$$

$$\psi_{0,0;1}^4 = \frac{1}{2\sqrt{4!}} \left[\left| \phi_1 \bar{\phi}_2 \phi_3 \bar{\phi}_4 \right| - \left| \phi_1 \bar{\phi}_2 \bar{\phi}_3 \phi_4 \right| - \left| \bar{\phi}_1 \phi_2 \phi_3 \bar{\phi}_4 \right| + \left| \bar{\phi}_1 \phi_2 \bar{\phi}_3 \phi_4 \right| \right], \quad (65)$$

$$\psi_{0,0;2}^4 = \frac{1}{2\sqrt{4!}} \left[\left| \phi_1 \phi_2 \bar{\phi}_3 \bar{\phi}_4 \right| - \left| \phi_1 \bar{\phi}_2 \phi_3 \bar{\phi}_4 \right| - \left| \bar{\phi}_1 \phi_2 \bar{\phi}_3 \phi_4 \right| + \left| \bar{\phi}_1 \bar{\phi}_2 \phi_3 \phi_4 \right| \right]. \quad (66)$$

Thus, for H_4 in a singlet state, the SCGVB wavefunction is written as a two-structure expansion in a basis of four spin-coupled orbitals. The variational optimization of c_1 , c_2 , and the orbitals $\{\phi_i\}$ proceeds by minimizing Eq. (17), which in practice requires the evaluation of Hamiltonian and overlap matrix elements between the determinants appearing in Eqs. (65)–(66) [3, 29].

$$\begin{aligned}\tilde{\Psi}_{\text{SCGVB}} &= c_1 \left[\left| \chi_1 \bar{\chi}_2 \chi_3 \bar{\chi}_4 \right| - \left| \chi_1 \bar{\chi}_2 \bar{\chi}_3 \chi_4 \right| - \left| \bar{\chi}_1 \chi_2 \chi_3 \bar{\chi}_4 \right| + \left| \bar{\chi}_1 \chi_2 \bar{\chi}_3 \chi_4 \right| \right] \\ &\quad + c_2 \left[\left| \chi_1 \chi_2 \bar{\chi}_3 \bar{\chi}_4 \right| - \left| \chi_1 \bar{\chi}_2 \chi_3 \bar{\chi}_4 \right| - \left| \bar{\chi}_1 \chi_2 \bar{\chi}_3 \chi_4 \right| + \left| \bar{\chi}_1 \bar{\chi}_2 \chi_3 \chi_4 \right| \right], \quad (67)\end{aligned}$$

which is formally a traditional valence bond wavefunction built from a fixed set of localized orbitals. In this simplified setting, one may focus exclusively on the evaluation (classically or on a quantum device) of the Hamiltonian and overlap matrix elements between the determinants in Eqs. (65)–(66), use them to construct the 2×2 Hamiltonian and overlap matrices in the $\{\psi_{0,0;1}^4, \psi_{0,0;2}^4\}$ basis, and finally solve the generalized eigenvalue problem to obtain the SCGVB coefficients (c_1, c_2) and the ground-state energy of H_4 .

$$\Theta_{0,0;2}^4 = \frac{1}{\sqrt{2}} \left(\alpha_1 \beta_4 - \beta_1 \alpha_4 \right) \frac{1}{\sqrt{2}} \left(\alpha_2 \beta_3 - \beta_2 \alpha_3 \right), \quad (64)$$

where $\alpha_i \equiv \alpha(\sigma_i)$ and $\beta_i \equiv \beta(\sigma_i)$. Expanding these products in primitive spin functions and applying the antisymmetrizer yields the corresponding spin-coupled structures as linear combinations of Slater determinants. Using the shorthand $\phi_i(\mathbf{x}) = \phi_i(\mathbf{r})\alpha(\sigma)$ and $\bar{\phi}_i(\mathbf{x}) = \phi_i(\mathbf{r})\beta(\sigma)$, the two spin-coupled structures can be compactly expressed as

A useful simplification, particularly in the context of testing quantum algorithms or approximate treatments, is to freeze the spin-coupled orbitals and identify them with a minimal set of atomic basis functions for H_4 , e.g. the four $1s$ functions of an STO-3G basis. Denoting these fixed orbitals by $\chi_1, \chi_2, \chi_3, \chi_4$, the approximate SCGVB wavefunction becomes

This H_4 model provides a minimal yet nontrivial testbed for SCGVB theory, for Chirgwin–Coulson weight analysis, and for exploring alternative strategies (including quantum computing) to handle the nonorthogonal determinant algebra that underpins modern valence bond methods.

V. RESULTS

To assess the operational feasibility of the proposed SCGVB quantum estimators, we consider the H_4 cluster.

A. H_4 cluster

The H_4 system serves as a minimal yet nontrivial test case, featuring strong static correlation and qualitative changes in the bonding pattern along the dissociation coordinate. For this system, the full overlap and Hamiltonian matrices were evaluated using the Pauli-grouped Hamiltonian estimator, demonstrating the complete ancilla-free and shallow-circuit workflow of the method.

a. Accuracy of the quantum-estimated Hamiltonian. To assess the accuracy of the proposed measurement-only quantum algorithm, we compared the complete SCGVB Hamiltonian matrix H^{QA} obtained on the quantum circuit emulator with the classical reference matrix H^{ref} . The absolute elemental deviation is defined as $|\Delta H_{ij}| = |H_{ij}^{\text{QA}} - H_{ij}^{\text{ref}}|$. The full deviation matrix for the square H_4 geometry is reported in Table I. The complete information about the other geometries used in these results is provided in the Appendix D.

Importantly, the observed deviations do not preferentially affect any specific class of matrix elements, indicating that the measurement-only estimator preserves the relative structure of the nonorthogonal Hamiltonian rather than introducing systematic bias. This property is essential for the stability of generalized eigenvalue problems involving strongly overlapping determinant bases.

b. Accuracy of the quantum-estimated overlap matrix. Because a minimal basis is employed, the present results do not aim at chemical accuracy with respect to the complete basis set limit, but rather at validating the accuracy of the quantum algorithm within a fixed orbital representation. Table II reports the full overlap matrix between the six nonorthogonal SCGVB determinants for the square H_4 geometry. The agreement between the quantum-estimated overlaps obtained from the Determinant–Overlap Estimator (DOE) and the classical values computed using Löwdin’s nonorthogonal determinant rules is essentially exact, with absolute discrepancies on the order of 10^{-9} or smaller. This level of agreement validates both the nonorthogonal Jordan–Wigner mapping and the measurement protocol used to reconstruct determinant overlaps from vacuum-projected Pauli strings.

From a physical perspective, the overlap matrix clearly reflects the strongly nonorthogonal character of the SCGVB determinant basis at the square geometry. Several off-diagonal elements are sizable, indicating significant interference between distinct valence-bond pairing patterns enforced by the high symmetry of the cluster. This nonorthogonality is intrinsic to the SCGVB description and cannot be eliminated without altering the phys-

ical content of the wavefunction. The ability of the quantum algorithm to reproduce these overlap patterns with high fidelity is therefore a nontrivial requirement for the stability of the generalized eigenvalue problem.

Overall, the agreement between quantum and classical matrix elements is excellent. The maximum deviation observed is $\max_{i,j} |\Delta H_{ij}| = 3.30 \times 10^{-2}$ Ha, which occurs on a diagonal element. This behavior is expected, as diagonal matrix elements involve larger absolute Hamiltonian expectation values and accumulate contributions from a greater number of Pauli terms, rendering them statistically more sensitive to finite-shot noise than off-diagonal couplings. Most off-diagonal contributions exhibit significantly smaller deviations, typically in the range 10^{-3} – 10^{-2} Ha, and several elements fall below 3×10^{-4} Ha. Such fluctuations are fully consistent with statistical noise due to finite sampling: each matrix element corresponds to a weighted sum of thousands of Pauli-term expectation values, each estimated using 5.24×10^5 measurement shots. The deviations appear randomly distributed across diagonal and off-diagonal sectors, with no discernible systematic trend, suggesting that the quantum reconstruction does not introduce a dominant bias beyond statistical noise. From a physical perspective, the magnitude of these errors is sufficiently small to guarantee a stable recovery of the SCGVB ground-state energy via the generalized eigenvalue problem $Hc = ESc$. The largest deviation (0.033 Ha), although prominent at the matrix-element level, represents roughly 0.2% of the diagonal entry’s magnitude, and its effect is moderated when solving the full nonorthogonal eigenvalue problem. These results demonstrate that the measurement-only architecture—comprising only single-qubit basis rotations and measurements, and requiring no entangling gates—is capable of accurately reconstructing a correlated many-electron Hamiltonian. Solving the generalized eigenvalue problem using the quantum-estimated Hamiltonian and overlap matrices yields a ground-state energy in excellent agreement with the classical Löwdin reference. Across all geometries considered, the resulting energy deviation remains well below the intrinsic matrix-element fluctuations induced by finite sampling, confirming that the observed errors do not compromise the stability or physical reliability of the SCGVB solution.

c. Scope of quantum advantage and comparison with Hadamard tests. The present algorithm is not intended to demonstrate an asymptotic quantum advantage in the complexity-theoretic sense. Instead, its objective is to provide a resource-efficient and hardware-compatible strategy for evaluating SCGVB Hamiltonian and overlap matrix elements on near-term quantum devices. In particular, the proposed measurement-only estimators avoid the use of ancilla qubits, controlled unitaries, and deep circuits that are characteristic of standard Hadamard-test and modified Hadamard-test approaches. While Hadamard-based schemes can in principle evaluate the same matrix elements, they require circuit depths that

TABLE I: Hamiltonian matrix elements (in Hartree) between nonorthogonal SCGVB Slater determinants. Columns show the quantum-estimated matrix elements (PGHE quantum circuit), the classical Löwdin reference, and the absolute deviation $|\Delta H_{ij}|$. The target system is a square H_4 molecule 0.7444×0.7414 (Å). Only unique elements ($i \leq j$) are reported since the Hamiltonian matrix is Hermitian.

H_{ij}	Quantum Circuit	Löwdin reference	$ \Delta H_{ij} $
$\langle \psi_1 H \psi_1 \rangle$	-1.4174356874	-1.447215508	0.0297798206
$\langle \psi_1 H \psi_2 \rangle$	0.3223085002	0.318808565	0.0034999352
$\langle \psi_1 H \psi_3 \rangle$	0.3265732036	0.318808565	0.0077646386
$\langle \psi_1 H \psi_4 \rangle$	0.0111227864	0.01720101851	0.0060782321
$\langle \psi_1 H \psi_5 \rangle$	0.3185223847	0.318808565	0.0002861803
$\langle \psi_1 H \psi_6 \rangle$	0.3302189815	0.318808565	0.0114104160
$\langle \psi_2 H \psi_2 \rangle$	-0.6430841052	-0.6331848711	0.0098992341
$\langle \psi_2 H \psi_3 \rangle$	-0.1505910757	-0.1478321999	0.0027588758
$\langle \psi_2 H \psi_4 \rangle$	0.3091913045	0.318808565	0.0096172605
$\langle \psi_2 H \psi_5 \rangle$	-0.0090499437	-0.005690144139	0.0033597996
$\langle \psi_2 H \psi_6 \rangle$	-0.0075174089	-0.005690144139	0.0018272648
$\langle \psi_3 H \psi_3 \rangle$	-0.6594546921	-0.6331848711	0.0262698210
$\langle \psi_3 H \psi_4 \rangle$	0.3111067327	0.318808565	0.0077018323
$\langle \psi_3 H \psi_5 \rangle$	-0.0079179479	-0.005690144139	0.0022278038
$\langle \psi_3 H \psi_6 \rangle$	-0.0028908252	-0.005690144139	0.0027993189
$\langle \psi_4 H \psi_4 \rangle$	-1.4142364353	-1.447215508	0.0329790727
$\langle \psi_4 H \psi_5 \rangle$	0.3245050937	0.318808565	0.0056965287
$\langle \psi_4 H \psi_6 \rangle$	0.3281355396	0.318808565	0.0093269747
$\langle \psi_5 H \psi_5 \rangle$	-0.6364821722	-0.6331848711	0.0032973011
$\langle \psi_5 H \psi_6 \rangle$	-0.1488527680	-0.1478321999	0.0010205681
$\langle \psi_6 H \psi_6 \rangle$	-0.6417711786	-0.6331848711	0.0085863075

scale with the length of Pauli strings and the use of multi-qubit controlled operations, making them poorly suited for NISQ-era hardware. By contrast, the present approach relies exclusively on single-qubit Clifford gates and projective measurements, yielding constant-depth circuits independent of system size. Although this does not constitute a formal quantum speedup, the reduction in circuit depth, gate complexity, and qubit overhead represents a clear practical advantage for near-term implementations.

d. Quantum resource requirements. A detailed resource estimate for the Hamiltonian reconstruction is presented in Table III. Each Pauli group is measured using shallow circuits of depth 2, containing only single-qubit gates (H and S^\dagger) and projective measurements. No CNOT or other entangling gates are required, a consequence of the qubit-wise commuting grouping of Pauli operators. In total, 86,906 circuits were executed, corresponding to 42,102 one-body and 44,804 two-body contributions. Across all circuits, the peak memory footprint of the simulation was approximately 9.95 GB, and the total runtime was roughly 42,315 s. These data provide a realistic estimate of the classical resources required to simulate the measurement-based quantum algorithm for nonorthogonal SCGVB states, and establish a clear baseline for the scaling of the method beyond eight qubits.

e. Efficient encoding of SCGVB physics on NISQ hardware A key conceptual aspect of the present approach is that the SCGVB wavefunction itself is never prepared on the quantum device. All nonorthogonality, spin coupling, and configuration interaction coefficients

are handled classically, while the quantum processor is used solely to evaluate overlaps and Hamiltonian matrix elements between nonorthogonal determinants. As a result, the quantum circuits act only on the computational vacuum and never generate entanglement, despite encoding correlated many-electron physics.

This hybrid strategy enables an efficient realization of SCGVB theory within the constraints of NISQ hardware. The shallow circuit depths reported in Table III, together with the absence of entangling gates, indicate that the dominant limitation of the present implementation is statistical sampling rather than coherent quantum control. These features make the approach well suited for early fault-tolerant or high-fidelity NISQ devices, where measurement throughput is more readily available than long coherent gate sequences.

f. Chirgwin–Coulson weights and physical interpretation Because the Chirgwin–Coulson (CC) weights depend explicitly on both the generalized eigenvector coefficients and the nonorthogonal overlap matrix, they provide a stringent, physically meaningful test of the quality of the quantum-estimated Hamiltonian and overlap matrices. Unlike individual matrix elements, the CC weights are sensitive to correlated errors in H and S , and small inaccuracies in the overlap matrix can propagate nonlinearly into unphysical weights (e.g., negative values or weights exceeding unity). As shown in Table IV and Fig. 4, the CC weights obtained from the quantum-estimated matrices reproduce the expected chemical behavior along the $H_4 \rightarrow H_2 + H_2$ dissociation coordinate. At the square geometry, symmetry enforces

TABLE II: Overlap matrix elements between the six SCGVB determinants. The column “QA (DOE)” lists the values obtained from the quantum circuit, while “Löwdin rules” contains the classical reference. Absolute discrepancies are $|\Delta S_{ij}| = |S_{ij}^{\text{QA}} - S_{ij}^{\text{ref}}|$. Only unique elements ($i \leq j$) are reported since the overlap matrix is symmetric.

S_{ij}	QA (DOE)	Löwdin rules	$ \Delta S_{ij} $
$\langle \psi_1 \psi_1 \rangle$	0.6093766053	0.6093766115	6.2×10^{-9}
$\langle \psi_1 \psi_2 \rangle$	-0.1227232093	-0.1227232103	1.0×10^{-9}
$\langle \psi_1 \psi_3 \rangle$	-0.1227232093	-0.1227232103	1.0×10^{-9}
$\langle \psi_1 \psi_4 \rangle$	0.0000000000	0.0000000000	0
$\langle \psi_1 \psi_5 \rangle$	-0.1227232093	-0.1227232103	1.0×10^{-9}
$\langle \psi_1 \psi_6 \rangle$	-0.1227232093	-0.1227232103	1.0×10^{-9}
$\langle \psi_2 \psi_2 \rangle$	0.3201019318	0.3201019355	3.7×10^{-9}
$\langle \psi_2 \psi_3 \rangle$	0.0461606361	0.0461606364	3.0×10^{-10}
$\langle \psi_2 \psi_4 \rangle$	-0.1227232093	-0.1227232103	1.0×10^{-9}
$\langle \psi_2 \psi_5 \rangle$	-0.0011661906	-0.0011661905	1.0×10^{-10}
$\langle \psi_2 \psi_6 \rangle$	-0.0011661906	-0.0011661905	1.0×10^{-10}
$\langle \psi_3 \psi_3 \rangle$	0.3201019318	0.3201019355	3.7×10^{-9}
$\langle \psi_3 \psi_4 \rangle$	-0.1227232093	-0.1227232103	1.0×10^{-9}
$\langle \psi_3 \psi_5 \rangle$	-0.0011661906	-0.0011661905	1.0×10^{-10}
$\langle \psi_3 \psi_6 \rangle$	-0.0011661906	-0.0011661905	1.0×10^{-10}
$\langle \psi_4 \psi_4 \rangle$	0.6093766053	0.6093766115	6.2×10^{-9}
$\langle \psi_4 \psi_5 \rangle$	-0.1227232093	-0.1227232103	1.0×10^{-9}
$\langle \psi_4 \psi_6 \rangle$	-0.1227232093	-0.1227232103	1.0×10^{-9}
$\langle \psi_5 \psi_5 \rangle$	0.3201019318	0.3201019355	3.7×10^{-9}
$\langle \psi_5 \psi_6 \rangle$	0.0461606361	0.0461606364	3.0×10^{-10}
$\langle \psi_6 \psi_6 \rangle$	0.3201019318	0.3201019355	3.7×10^{-9}

TABLE III: Quantum resource summary for the evaluation of the SCGVB Hamiltonian matrix elements of square H_4 .

Quantity	Value
Number of spatial orbitals	4
Number of spin-orbitals	8
Number of qubits	8
Total circuits (one-body Hamiltonian)	42 102
Total circuits (two-body Hamiltonian)	44 804
Total circuits (all contributions)	86 906
Average circuit depth	2
Maximum circuit depth	2
Average gate count per circuit	13–14
Maximum gate count per circuit	16
Total H gates (one-body)	120 372
Total U2 gates (one-body)	120 372
Total measurements (one-body)	336 816
Total H gates (two-body)	125 488
Total U2 gates (two-body)	125 488
Total measurements (two-body)	358 432
Total simulation time (one-body)	19 558.46 s
Total simulation time (two-body)	22 756.78 s
Peak memory (tracemalloc)	9.95 GB
Shots per circuit	524 288

equal contributions of the two spin-coupled structures ($w_1 = w_2 = 0.5$), which is accurately recovered by the quantum algorithm. Upon elongation of one H–H distance, the weights evolve smoothly and monotonically, with one structure becoming dominant as the system approaches two separated H_2 fragments. No negative or anomalously large weights are observed, indicating that

TABLE IV: **Bond-Breaking Signatures from Chirgwin–Coulson Weights** - c_1 , c_2 and CC weights w_1 , w_2 for the dissociation path of $H_4 \rightarrow H_2 + H_2$. Geometries are given as the two H–H distances (in Å) defining the rectangular H_4 cluster.

Geometry (Å)	c_1	c_2	w_1	w_2
0.7444×0.7414	-0.3122	0.3122	0.5000	0.5000
0.8800×0.7414	-0.0887	0.4481	0.2618	0.7382
0.92675×0.7414	-0.0560	0.4518	0.2021	0.7978
1.2000×0.7414	-0.0018	0.4402	0.0136	0.9863
1.2600×0.7414	0.0000	0.4000	0.0000	1.0000

the quantum-estimated overlap matrix preserves the delicate balance required for a stable CC analysis.

Because the Chirgwin–Coulson weights depend nonlinearly on both the Hamiltonian and overlap matrices, their smooth and physically consistent behavior constitutes a stringent validation of the quantum algorithm’s ability to preserve nonorthogonal interference effects beyond individual matrix-element accuracy.

The close agreement with CC weights obtained from classical Löwdin-rule calculations demonstrate that the proposed measurement-only quantum approach is capable not only of reproducing individual matrix elements, but also of faithfully capturing derived, chemically interpretable quantities that depend on the full nonorthogonal structure of the SCGVB problem.

Overall, Table V shows that the quantum-estimated Hamiltonian reproduces the classical Löwdin reference with sub- 10^{-2} Hartree mean absolute error across all geometries considered. The largest deviations consistently

TABLE V: Summary of absolute deviations between quantum-circuit and Löwdin-reference Hamiltonian matrix elements for square and rectangular H_4 geometries. Statistics are computed over all 36 matrix elements:

$$\text{Mean } |\Delta H| = \frac{1}{36} \sum_{ij} |\Delta H_{ij}|, \text{ RMS } |\Delta H| = \sqrt{\frac{1}{36} \sum_{ij} |\Delta H_{ij}|^2}, \text{ and Max } |\Delta H| = \max_{ij} |\Delta H_{ij}|.$$

Geometry (Å)	Mean $ \Delta H $ (Ha)	RMS $ \Delta H $ (Ha)	Max $ \Delta H $ (Ha)	Argmax (i, j)
0.7414×0.7414	0.0079	0.0115	0.03298	(4,4)
0.7414×0.88	0.0075	0.0109	0.03336	(1,1)
0.7414×0.92675	0.0066	0.0095	0.03111	(4,4)
0.7414×1.20	0.0055	0.0079	0.02338	(3,3)
0.7414×1.26	0.0060	0.0085	0.02739	(4,4)

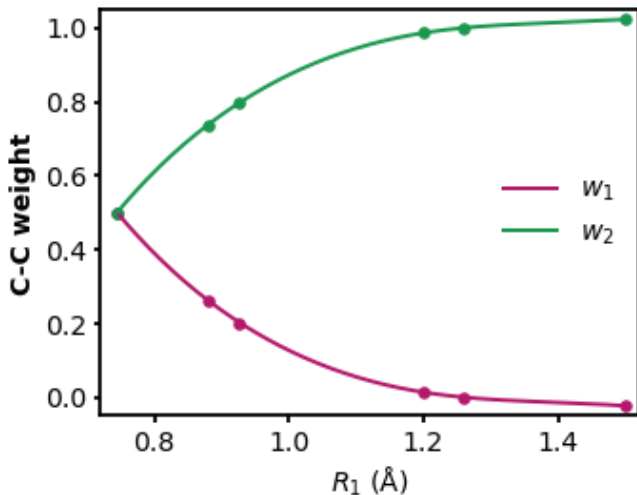


FIG. 4: Chirgwin–Coulson weights w_1 and w_2 for the two SCGVB structures of H_4 along the $H_4 \rightarrow H_2 + H_2$ dissociation coordinate.

arising from the diagonal matrix elements corresponding to strongly interacting configurations.

Unlike individual Hamiltonian or overlap matrix elements, the Chirgwin–Coulson weights probe the global consistency of the quantum-estimated matrices. Their smooth and physically correct behavior therefore demonstrates not merely numerical accuracy, but the preservation of nonorthogonal interference effects that are central to valence-bond theory.

Taken together, these results demonstrate that, while the proposed algorithm does not offer a formal quantum advantage, it provides a practically attractive and conceptually transparent route to evaluating nonorthogonal SCGVB matrices. elements using shallow, measurement-only quantum circuits, with quantitative accuracy matching classical Löwdin-rule calculations.

Although the present work is motivated by near-term hardware considerations, the proposed measurement-only estimators are fully compatible with fault-tolerant quantum architectures, as they rely exclusively on single-qubit Clifford operations and projective measurements.

Taken together, the H_4 results demonstrate that the proposed Measurement-only estimators reliably reproduce both the numerical and physical structure of the SCGVB problem across distinct bonding regimes, using

only shallow, ancilla-free quantum circuits.

The implementation details for this system are provided in Appendices B and C.

VI. CONCLUSION AND OUTLOOK

We have presented a quantum measurement framework for evaluating overlap and Hamiltonian matrix elements in nonorthogonal SCGVB wavefunctions. By recasting the required quantities as vacuum expectation values of Pauli-string operators, the method replaces direct manipulation of nonorthogonal wavefunctions on hardware with ancilla-free, shallow measurement circuits built from local Clifford rotations and computational-basis readout. This provides a hardware-compatible route for integrating quantum measurements into SCGVB workflows while preserving the chemically transparent structure of valence-bond theory.

Tests on square and rectangular H_4 show that the quantum-estimated overlap and Hamiltonian matrices agree well with classical Löwdin-based references across the geometries considered. In addition, the derived Coulson–Chirgwin weights remain consistent with the underlying chemical picture, indicating that the estimated matrix elements retain meaningful physical information rather than merely reproducing isolated numerical entries. Taken together, these results demonstrate the practical viability of measurement-based quantum assistance for nonorthogonal valence-bond calculations.

At the same time, the scope of the present contribution should be stated clearly. The method does not establish an asymptotic quantum advantage, and the classical preprocessing associated with SCGVB algebra remains essential. Its principal value is instead practical: reducing hardware demands by avoiding preparation of the full nonorthogonal ansatz, controlled operations, and deep circuits, while relying on simple measurement primitives that are more naturally aligned with near-term quantum devices.

A natural direction for future work is the extension of the present framework beyond H_4 to larger molecular systems. Preliminary tests on C_2 indicate that the current implementation based on the nonorthogonal Jordan–Wigner (NO-JW) [12] mapping becomes computationally prohibitive at this scale, as the associated classical preprocessing exceeded practical multi-day supercom-

puting times. This suggests that, although the present NO-JW workflow is effective for systems such as H_4 , it is not suitable in its current form for larger molecules within the SCGVB framework. A more scalable treatment of systems such as C_2 will likely require a reformulation in which the nonorthogonal mapping is incorporated more directly into the quantum circuit, rather than handled through the present preprocessing strategy. Developing such a circuit-native extension, together with a broader analysis of scaling and resource requirements relative to alternative overlap- and Hamiltonian-estimation schemes, constitutes an important direction for future work. Within that scope, the present results provide a concrete step toward hardware-assisted valence-bond quantum chemistry.

ACKNOWLEDGMENTS

The Italian Research Center on High Performance Computing, Big Data, and Quantum Computing (ICSC) is acknowledged for financial support under the Innovation Grant Project “Molecular Energy Landscapes by Quantum Computing.

REFERENCES

- [1] B. Chirgwin and C. A. Coulson, “The electronic structure of conjugated systems. VI. The evaluation of valence bond structures and resonance energies,” *Proc. R. Soc. A* **201**, 196 (1950).
- [2] P. O. Löwdin, “On the non-orthogonality problem connected with the use of atomic wave functions in the theory of molecules and crystals,” *J. Chem. Phys.* **18**, 365 (1950).
- [3] T. Thorsteinsson, *Development of Methods in Spin-Coupled Theory*, Ph.D. Thesis, University of Liverpool (1995).
- [4] S. Shaik and P. C. Hiberty, “Valence Bond Theory: Its History, Fundamentals, and Applications—A Primer,” *Chem. Rev.* **112**, 2027 (2012).
- [5] F. E. Penotti, J. N. Murrell, and M. J. Yates, “Spin-Coupled GVB Descriptions of π -Electron Systems in S_2N_2 and $S_4N_4^{2+}$ Rings,” *J. Chem. Phys.* **150**, 204302 (2019).
- [6] B. G. M. Araújo and A. M. S. Macedo, “Compactifying Electronic Wavefunctions I: Error-Mitigated Transcorrelated DMRG,” arXiv:2503.00627 [quant-ph], 2025. Available at: <https://arxiv.org/abs/2503.00627>.
- [7] *Chirgwin–Coulson weights*, Wikipedia, accessed November 2025, https://en.wikipedia.org/wiki/Chirgwin%E2%80%9E93Coulson_weights.
- [8] R. McWeeny, *Methods of Molecular Quantum Mechanics*, 2nd ed. (Academic Press, London, 1992).
- [9] R. Pauncz, *Spin Eigenfunctions: Construction and Use* (Plenum Press, New York, 1979).
- [10] B. G. M. Araújo, M. M. Taddei, D. Cavalcanti, and A. Acín, “Local quantum overlapping tomography,” *Phys. Rev. A* **106**, 062441 (2022). doi:10.1103/PhysRevA.106.062441.
- [11] A. Pérez-Obiol, A. Pérez-Salinas, S. Sánchez-Ramírez, B. G. M. Araújo, and A. Garcia-Saez, “Adiabatic quantum algorithm for artificial graphene,” *Phys. Rev. A* **106**, 052408 (2022). doi:10.1103/PhysRevA.106.052408.
- [12] A. Marruzzo, M. Casalegno, P. Macchia, F. Mascherpa, B. Tirri, G. Raos, and A. Genoni, “Extension of the Jordan–Wigner mapping to nonorthogonal spin orbitals for quantum computing: application to valence bond approaches,” in *A Snapshot of Molecular Electronic Structure Theory and its Applications*, Elsevier, 2025, pp. 245–266. doi: 10.1016/bs.aicq.2025.07.007.
- [13] D. Gottesman, *The Heisenberg Representation of Quantum Computers*, in *Proceedings of the XXII International Colloquium on Group Theoretical Methods in Physics*, Cambridge, MA, 1998, arXiv:quant-ph/9807006.
- [14] S. Aaronson and D. Gottesman, *Improved Simulation of Stabilizer Circuits*, *Phys. Rev. A* **70**, 052328 (2004).
- [15] P. O. Löwdin, “Quantum theory of many-particle systems. I. Physical interpretations by means of density matrices, natural spin-orbitals, and convergence problems in the method of configurational interaction,” *Phys. Rev.* **97**, 1474 (1955).
- [16] P. O. Löwdin, “Studies in perturbation theory. IV. Solution of eigenvalue problem by projection operator formalism,” *J. Math. Phys.* **3**, 969 (1956).
- [17] W. A. Goddard III, T. H. Dunning Jr., W. J. Hunt, and P. J. Hay, “Generalized valence bond description of bonding in low-lying states of molecules,” *Acc. Chem. Res.* **6**, 368 (1973).
- [18] P. C. Hiberty and S. Shaik, “Comment on the relationship between valence bond and molecular orbital methods,” *J. Comput. Chem.* **23**, 973 (2002).
- [19] W. Kutzelnigg and D. Mukherjee, “Normal Order and Extended Wick Theorem for a Multiconfiguration Reference Wave Function,” *J. Chem. Phys.* **1997**, 107, 432–449. DOI: 10.1063/1.474405.
- [20] Shaik, S.; Hiberty, P. C. *A Chemist’s Guide to Valence Bond Theory*; John Wiley & Sons, Inc.: Hoboken, NJ, 2007; DOI: 10.1002/9780470192597.
- [21] A. Szabo and N. S. Ostlund, *Modern Quantum Chemistry: Introduction to Advanced Electronic Structure Theory*, Dover Publications, New York (1996).
- [22] T. Helgaker, P. Jørgensen, and J. Olsen, *Molecular Electronic-Structure Theory*, Wiley, Chichester (2000).
- [23] R. Cleve, A. Ekert, C. Macchiavello, and M. Mosca, *Quantum Algorithms Revisited*, *Proc. R. Soc. A* **454**, 339–354 (1998). <https://doi.org/10.1098/rspa.1998.0164>
- [24] A. Yu. Kitaev, *Quantum Measurements and the Abelian Stabilizer Problem*, in *Proceedings of the 22nd International Colloquium on Group Theoretical Methods in Physics*, Cambridge, MA, 1997; arXiv:quant-ph/9511026.

- [25] M. A. Nielsen and I. L. Chuang, *Quantum Computation and Quantum Information*, Cambridge University Press, Cambridge, 2010.
- [26] U. Baek, D. Hait, J. Shee, O. Leimkuhler, W. J. Huggins, T. F. Stetina, M. Head-Gordon, and K. B. Whaley, *Say NO to Optimization: A Nonorthogonal Quantum Eigensolver*, PRX Quantum **4**, 030307 (2023). <https://doi.org/10.1103/PRXQuantum.4.030307>
- [27] Q. Sun, T. C. Berkelbach, N. S. Blunt, *et al.*, “PySCF: the Python-based simulations of chemistry framework,” *WIREs Comput. Mol. Sci.* **8**, e1340 (2018).
- [28] H. Abraham *et al.*, “Qiskit: An Open-source Framework for Quantum Computing,” Zenodo, 2019. DOI: 10.5281/zenodo.2562111.
- [29] T. H. Dunning, Jr., L. T. Xu, D. L. Cooper, and P. B. Karadakov, “Spin-Coupled Generalized Valence Bond Theory: New Perspectives on the Electronic Structure of Molecules and Chemical Bonds,” *J. Phys. Chem. A* **125**, 2021–2050 (2021).
- [30] T. H. Dunning, Jr., D. L. Cooper, L. T. Xu, and P. B. Karadakov, “Spin-Coupled Generalized Valence Bond Theory: An Appealing Orbital Theory of the Electronic Structure of Atoms and Molecules,” in *Comprehensive Computational Chemistry, Vol. 1: Valence Bond (VB) Theory and Related Approaches*, edited by S. Shaik and P. C. Hiberty (Elsevier, 2023), pp. V1-354–V1-402.
- [31] D. L. Cooper, “Valence Bond Theory: Introduction to *Ab Initio* Modern VB Methods,” Lecture Notes (Sorbonne/LCT Workshop, 2014).
- [32] D. L. Cooper, J. Gerratt, and M. Raimondi, “The spin-coupled valence bond theory of molecular electronic structure,” *Adv. Chem. Phys.* **69**, 319–397 (1987).
- [33] G. D. Fletcher, M. W. Schmidt, and M. S. Gordon, “Valence: A Massively Parallel Implementation of the Spin-Coupled Generalized Valence Bond Method,” *J. Comput. Chem.* **40**, 1119–1131 (2019).
- [34] G. Rumer, “Zur Theorie der Spinvalenz,” *Nachrichten von der Gesellschaft der Wissenschaften zu Göttingen, Mathematisch-Physikalische Klasse* **1932**, 337–341 (1932).
- [35] G. Raos, J. Gerratt, D. L. Cooper, and M. Raimondi, “On the role of different spin bases within spin-coupled theory,” *Mol. Phys.* **79**, 197–216 (1993). doi: [10.1080/00268979300101151](https://doi.org/10.1080/00268979300101151).
- [36] L.-T. Xu and T. H. Dunning, Jr., “Insights into the Perplexing Nature of the Bonding in C_2 from Generalized Valence Bond Calculations,” *J. Chem. Theory Comput.* **10**, 195–201 (2014). doi: [10.1021/ct400867h](https://doi.org/10.1021/ct400867h).
- [37] D. L. Cooper, F. E. Penotti, and R. Ponec, “Why is the bond multiplicity in C_2 so elusive?” *Comput. Theor. Chem.* **1053**, 189–194 (2015). doi: [10.1016/j.comptc.2014.08.024](https://doi.org/10.1016/j.comptc.2014.08.024).
- [38] G. Raos, J. Gerratt, D. L. Cooper, and M. Raimondi, “Spin correlation in π -electron systems from spin-coupled wavefunctions. II. Further applications,” *Chem. Phys.* **186**, 251–273 (1994). doi: [10.1016/0301-0104\(94\)00178-2](https://doi.org/10.1016/0301-0104(94)00178-2).

Appendix A: Implementation details of the nonorthogonal Jordan–Wigner encoding

Here we implemented the NOJW mapping proposed by [12] using Qiskit. To assess the correctness of the proposed Jordan-Wigner encoding in the nonorthogonal case, the mappings given by Eq. 47 for the operator $\{\hat{a}_p\}$. The implementation is conceptually straightforward. In our case, the challenge stands in the mapping of the $\{\hat{a}_p\}$ operators corresponding to nonorthogonal spin orbitals. To illustrate this concretely, below we present a Python routine snippet that uses the `SparsePauliOp` object from Qiskit to represent a nonorthogonal operator.

```

1 from qiskit.quantum_info import SparsePauliOp
2 import numpy as np
3
4 def nonorthogonal_annihilation_jw(p: int, S: np.ndarray) -> SparsePauliOp:
5     """
6     Returns the SparsePauliOp corresponding to the nonorthogonal JW mapping
7     of the annihilation operator a_p, using the overlap matrix S.
8     """
9     M = S.shape[0]
10    terms = []
11
12    for q in range(M):
13        coeff = S[p, q] / 2 # (X + iY)/2 has two parts
14        pauli_x = ['I'] * M
15        pauli_y = ['I'] * M
16        for k in range(q):
17            pauli_x[k] = 'Z'
18            pauli_y[k] = 'Z'
19        pauli_x[q] = 'X'
20        pauli_y[q] = 'Y'
21        # Add real and imaginary parts separately
22        terms.append((coeff, ''.join(pauli_x)))
23        terms.append((1j * coeff, ''.join(pauli_y)))
24
25    return SparsePauliOp.from_list(terms)
26 # -----
27 #Example
28 # -----
29 # Define a 4-orbital overlap matrix S (symmetric, real)
30 S = np.array([
31     [1.0, 0.2, 0.1, 0.05],
32     [0.2, 1.0, 0.3, 0.15],
33     [0.1, 0.3, 1.0, 0.25],
34     [0.05, 0.15, 0.25, 1.0]
35 ])
36 # Choose the index p for the annihilation operator a_p
37 p = 2 # for example, a_2 (third orbital)
38 # Get SparsePauliOp corresponding to a_2 under the NO JW mapping
39 a2_operator = nonorthogonal_annihilation_jw(p, S)
40 # Print the output
41 print("Nonorthogonal JW mapping for annihilation operator a_2:\n")
42 for label, coeff in a2_operator.to_list():
43     print(f"{coeff.real:.6f}{'+' if coeff.imag >= 0 else ''}{coeff.imag:.6f}j * {label}")

```

Listing 1: General NO-JW Mapping

In particular, to obtain the nonorthogonal Jordan-Wigner (JW) mapping for the fermionic operators $\{\hat{a}_p\}$, we implemented a general function that takes as input the index p of the operator \hat{a}_p and the spin orbital overlap matrix \mathbf{S} . The mapping constructs the Pauli operator representation of \hat{a}_p with S_{pq} being the weight as prescribed by Eq. 47. In the example above, we defined a 4×4 symmetric spin orbital overlap matrix and determined the mapped operator for \hat{a}_2 . The output consists of the complete Pauli decomposition, expressed as a sum of complex-weighted Pauli strings, which can be directly used in quantum simulations of nonorthogonal wavefunctions. This example highlights the general applicability of the proposed encoding beyond system-specific implementations.

Appendix B: Supplementary material about the implementation of SCGVB wavefunction for H_4 cluster

This appendix provides explicit operator-level details that are not required for understanding the conceptual workflow of the algorithm, but are included to ensure full reproducibility.

1. Spin-coupled SCGVB structures in second quantization

We provide explicit second-quantized expressions for the two spin-adapted SCGVB structures used in the main text. Let $|\phi_0\rangle \equiv |00000000\rangle$ denote the computational vacuum.

$$|\psi_{0,0;1}^4\rangle = \left(\hat{a}_1^\dagger \hat{a}_3^\dagger \hat{a}_6^\dagger \hat{a}_8^\dagger - \hat{a}_1^\dagger \hat{a}_4^\dagger \hat{a}_6^\dagger \hat{a}_7^\dagger - \hat{a}_2^\dagger \hat{a}_3^\dagger \hat{a}_5^\dagger \hat{a}_8^\dagger + \hat{a}_2^\dagger \hat{a}_4^\dagger \hat{a}_5^\dagger \hat{a}_7^\dagger \right) |\phi_0\rangle, \quad (\text{B1})$$

$$|\psi_{0,0;2}^4\rangle = \left(\hat{a}_1^\dagger \hat{a}_2^\dagger \hat{a}_7^\dagger \hat{a}_8^\dagger - \hat{a}_1^\dagger \hat{a}_3^\dagger \hat{a}_6^\dagger \hat{a}_8^\dagger - \hat{a}_2^\dagger \hat{a}_4^\dagger \hat{a}_5^\dagger \hat{a}_7^\dagger + \hat{a}_3^\dagger \hat{a}_4^\dagger \hat{a}_5^\dagger \hat{a}_6^\dagger \right) |\phi_0\rangle. \quad (\text{B2})$$

The SCGVB wavefunction is

$$|\psi_{\text{SCGVB}}\rangle = c_1 |\psi_{0,0;1}^4\rangle + c_2 |\psi_{0,0;2}^4\rangle. \quad (\text{B3})$$

2. Computational-basis (bitstring) representation

Using the occupation-number encoding in the main text, the same states can be written as

$$|\psi_{0,0;1}^4\rangle = (|10100101\rangle - |10010110\rangle - |01101001\rangle + |01011010\rangle), \quad (\text{B4})$$

$$|\psi_{0,0;2}^4\rangle = (|11000011\rangle - |10100101\rangle - |01011010\rangle + |00111100\rangle). \quad (\text{B5})$$

3. Determinant labels

For compactness we define the six determinants:

$$\begin{aligned} |\psi_1\rangle &= |10100101\rangle, & |\psi_2\rangle &= |10010110\rangle, & |\psi_3\rangle &= |01101001\rangle, \\ |\psi_4\rangle &= |01011010\rangle, & |\psi_5\rangle &= |11000011\rangle, & |\psi_6\rangle &= |00111100\rangle. \end{aligned} \quad (\text{B6})$$

In this notation,

$$|\psi_{0,0;1}^4\rangle = (|\psi_1\rangle - |\psi_2\rangle - |\psi_3\rangle + |\psi_4\rangle), \quad (\text{B7})$$

$$|\psi_{0,0;2}^4\rangle = (|\psi_5\rangle - |\psi_1\rangle - |\psi_4\rangle + |\psi_6\rangle). \quad (\text{B8})$$

Appendix C: Reduction of overlaps and Hamiltonian elements to vacuum expectation values

1. Creation and annihilation strings

Define creation strings f_k and corresponding annihilation strings w_k by

$$\begin{aligned} f_1 &= \hat{a}_1^\dagger \hat{a}_3^\dagger \hat{a}_6^\dagger \hat{a}_8^\dagger, & w_1 &= \hat{a}_8 \hat{a}_6 \hat{a}_3 \hat{a}_1, \\ f_2 &= \hat{a}_1^\dagger \hat{a}_4^\dagger \hat{a}_6^\dagger \hat{a}_7^\dagger, & w_2 &= \hat{a}_7 \hat{a}_6 \hat{a}_4 \hat{a}_1, \\ f_3 &= \hat{a}_2^\dagger \hat{a}_3^\dagger \hat{a}_5^\dagger \hat{a}_8^\dagger, & w_3 &= \hat{a}_8 \hat{a}_5 \hat{a}_3 \hat{a}_2, \\ f_4 &= \hat{a}_2^\dagger \hat{a}_4^\dagger \hat{a}_5^\dagger \hat{a}_7^\dagger, & w_4 &= \hat{a}_7 \hat{a}_5 \hat{a}_4 \hat{a}_2, \\ f_5 &= \hat{a}_1^\dagger \hat{a}_2^\dagger \hat{a}_7^\dagger \hat{a}_8^\dagger, & w_5 &= \hat{a}_8 \hat{a}_7 \hat{a}_2 \hat{a}_1, \\ f_6 &= \hat{a}_3^\dagger \hat{a}_4^\dagger \hat{a}_5^\dagger \hat{a}_6^\dagger, & w_6 &= \hat{a}_6 \hat{a}_5 \hat{a}_4 \hat{a}_3. \end{aligned} \quad (\text{C1})$$

Then each determinant is $|\psi_k\rangle = f_k |\phi_0\rangle$ and $\langle \psi_k | = \langle \phi_0 | w_k$.

2. Overlap matrix elements

All overlaps reduce to

$$S_{ij} = \langle \psi_i | \psi_j \rangle = \langle \phi_0 | w_i f_j | \phi_0 \rangle. \quad (\text{C2})$$

This form is the starting point for the measurement-only overlap estimator used in the main text.

3. Hamiltonian matrix elements

Similarly,

$$H_{ij} = \langle \psi_i | \hat{H} | \psi_j \rangle = \langle \phi_0 | w_i \hat{H} f_j | \phi_0 \rangle, \quad (\text{C3})$$

which is evaluated by expressing $w_i \hat{H} f_j$ as a weighted sum of Pauli strings under the (nonorthogonal) Jordan–Wigner mapping described in Appendix A.

4. NO-JW mapping of annihilation operators

For nonorthogonal spin-orbitals, the annihilation operator admits the expansion

$$\hat{a}_p = \sum_{q=1}^N S_{pq} \left(\prod_{k=1}^{q-1} Z_k \right) \frac{X_q + iY_q}{2}, \quad (\text{C4})$$

where S_{pq} are overlap matrix elements between spin-orbitals. For completeness, we list $\hat{a}_1, \dots, \hat{a}_8$ explicitly for the present 8-qubit problem:

$$\begin{aligned} \hat{a}_1 = & S_{11} \frac{X_1 + iY_1}{2} \otimes I_2 \otimes I_3 \otimes I_4 \otimes I_5 \otimes I_6 \otimes I_7 \otimes I_8 \\ & + S_{12} Z_1 \otimes \frac{X_2 + iY_2}{2} \otimes I_3 \otimes I_4 \otimes I_5 \otimes I_6 \otimes I_7 \otimes I_8 \\ & + S_{13} Z_1 \otimes Z_2 \otimes \frac{X_3 + iY_3}{2} \otimes I_4 \otimes I_5 \otimes I_6 \otimes I_7 \otimes I_8 \\ & + S_{14} Z_1 \otimes Z_2 \otimes Z_3 \otimes \frac{X_4 + iY_4}{2} \otimes I_5 \otimes I_6 \otimes I_7 \otimes I_8 \\ & + S_{15} Z_1 \otimes Z_2 \otimes Z_3 \otimes Z_4 \otimes \frac{X_5 + iY_5}{2} \otimes I_6 \otimes I_7 \otimes I_8 \\ & + S_{16} Z_1 \otimes Z_2 \otimes Z_3 \otimes Z_4 \otimes Z_5 \otimes \frac{X_6 + iY_6}{2} \otimes I_7 \otimes I_8 \\ & + S_{17} Z_1 \otimes Z_2 \otimes Z_3 \otimes Z_4 \otimes Z_5 \otimes Z_6 \otimes \frac{X_7 + iY_7}{2} \otimes I_8 \\ & + S_{18} Z_1 \otimes Z_2 \otimes Z_3 \otimes Z_4 \otimes Z_5 \otimes Z_6 \otimes Z_7 \otimes \frac{X_8 + iY_8}{2}. \end{aligned} \quad (\text{C5})$$

$$\begin{aligned} \hat{a}_2 = & S_{21} \frac{X_1 + iY_1}{2} \otimes I_2 \otimes I_3 \otimes I_4 \otimes I_5 \otimes I_6 \otimes I_7 \otimes I_8 \\ & + S_{22} Z_1 \otimes \frac{X_2 + iY_2}{2} \otimes I_3 \otimes I_4 \otimes I_5 \otimes I_6 \otimes I_7 \otimes I_8 \\ & + S_{23} Z_1 \otimes Z_2 \otimes \frac{X_3 + iY_3}{2} \otimes I_4 \otimes I_5 \otimes I_6 \otimes I_7 \otimes I_8 \\ & + S_{24} Z_1 \otimes Z_2 \otimes Z_3 \otimes \frac{X_4 + iY_4}{2} \otimes I_5 \otimes I_6 \otimes I_7 \otimes I_8 \\ & + S_{25} Z_1 \otimes Z_2 \otimes Z_3 \otimes Z_4 \otimes \frac{X_5 + iY_5}{2} \otimes I_6 \otimes I_7 \otimes I_8 \\ & + S_{26} Z_1 \otimes Z_2 \otimes Z_3 \otimes Z_4 \otimes Z_5 \otimes \frac{X_6 + iY_6}{2} \otimes I_7 \otimes I_8 \\ & + S_{27} Z_1 \otimes Z_2 \otimes Z_3 \otimes Z_4 \otimes Z_5 \otimes Z_6 \otimes \frac{X_7 + iY_7}{2} \otimes I_8 \\ & + S_{28} Z_1 \otimes Z_2 \otimes Z_3 \otimes Z_4 \otimes Z_5 \otimes Z_6 \otimes Z_7 \otimes \frac{X_8 + iY_8}{2}. \end{aligned} \quad (\text{C6})$$

TABLE VII: Hamiltonian matrix elements (in Hartree) between nonorthogonal SCGVB Slater determinants for rectangular H_4 ($0.88 \times 0.7414 \text{ \AA}$). Columns show the quantum-estimated matrix elements (PGHE quantum circuit), the classical Löwdin reference, and the absolute deviation $|\Delta H_{ij}|$. Only unique elements ($i \leq j$) are reported since the Hamiltonian matrix is Hermitian.

H_{ij}	Quantum Circuit	Löwdin reference	$ \Delta H_{ij} $
$\langle \psi_1 H \psi_1 \rangle$	-1.5541859494	-1.5841446083	0.0299586589
$\langle \psi_1 H \psi_2 \rangle$	0.2226076322	0.2190002768	0.0036073554
$\langle \psi_1 H \psi_3 \rangle$	0.2250376771	0.2190002768	0.0060374003
$\langle \psi_1 H \psi_4 \rangle$	-0.0233166916	-0.0233296753	0.0000129837
$\langle \psi_1 H \psi_5 \rangle$	0.4748015342	0.4695619606	0.0052395736
$\langle \psi_1 H \psi_6 \rangle$	0.4747209865	0.4695619606	0.0051590259
$\langle \psi_2 H \psi_2 \rangle$	-0.5933011243	-0.5846331188	0.0086680055
$\langle \psi_2 H \psi_3 \rangle$	-0.0762366273	-0.0738186226	0.0024180047
$\langle \psi_2 H \psi_4 \rangle$	0.2118894648	0.2190002768	0.0071108120
$\langle \psi_2 H \psi_5 \rangle$	-0.0054926232	-0.0049493105	0.0005433127
$\langle \psi_2 H \psi_6 \rangle$	-0.0041797147	-0.0049493105	0.0007695958
$\langle \psi_3 H \psi_3 \rangle$	-0.6081644331	-0.5846331188	0.0235313143
$\langle \psi_3 H \psi_4 \rangle$	0.2125972017	0.2190002768	0.0064030751
$\langle \psi_3 H \psi_5 \rangle$	-0.0053082375	-0.0049493105	0.0003589270
$\langle \psi_3 H \psi_6 \rangle$	-0.0037096120	-0.0049493105	0.0012396985
$\langle \psi_4 H \psi_4 \rangle$	-1.5508408075	-1.5841446083	0.0333038008
$\langle \psi_4 H \psi_5 \rangle$	0.4719640968	0.4695619606	0.0024021362
$\langle \psi_4 H \psi_6 \rangle$	0.4728043214	0.4695619606	0.0032423608
$\langle \psi_5 H \psi_5 \rangle$	-0.9475455136	-0.9390349435	0.0085105701
$\langle \psi_5 H \psi_6 \rangle$	-0.2243404939	-0.2205401655	0.0038003284
$\langle \psi_6 H \psi_6 \rangle$	-0.9494356410	-0.9390349435	0.0104006975

TABLE VIII: Overlap matrix elements between the six SCGVB determinants for rectangular H_4 ($0.88 \times 0.7414 \text{ \AA}$). The column “QA (DOE)” lists the values obtained from the quantum circuit, while “Löwdin rules” contains the classical reference. Absolute discrepancies are $|\Delta S_{ij}| = |S_{ij}^{\text{QA}} - S_{ij}^{\text{ref}}|$. Only unique elements ($i \leq j$) are reported since the overlap matrix is symmetric.

S_{ij}	QA (DOE)	Löwdin rules	$ \Delta S_{ij} $
$\langle \psi_1 \psi_1 \rangle$	0.6887973612	0.6887973612	0
$\langle \psi_1 \psi_2 \rangle$	-0.0887852187	-0.0887852187	0
$\langle \psi_1 \psi_3 \rangle$	0.0887852187	-0.0887852187	1.8×10^{-1}
$\langle \psi_1 \psi_4 \rangle$	0.0120235015	0.0120235015	0
$\langle \psi_1 \psi_5 \rangle$	-0.1797893730	-0.1797893730	0
$\langle \psi_1 \psi_6 \rangle$	-0.1797893730	-0.1797893730	0
$\langle \psi_2 \psi_2 \rangle$	0.3201019318	0.3201019318	0
$\langle \psi_2 \psi_3 \rangle$	0.0238736260	0.0238736260	0
$\langle \psi_2 \psi_4 \rangle$	-0.0887852187	-0.0887852187	0
$\langle \psi_2 \psi_5 \rangle$	-0.0013667206	-0.0013667206	0
$\langle \psi_2 \psi_6 \rangle$	-0.0013667206	-0.0013667206	0
$\langle \psi_3 \psi_3 \rangle$	0.3201019318	0.3201019318	0
$\langle \psi_3 \psi_4 \rangle$	0.0887852187	-0.0887852187	1.8×10^{-1}
$\langle \psi_3 \psi_5 \rangle$	-0.0013667206	-0.0013667206	2.7×10^{-3}
$\langle \psi_3 \psi_6 \rangle$	-0.0013667206	-0.0013667206	0
$\langle \psi_4 \psi_4 \rangle$	0.6887973612	0.6887973612	0
$\langle \psi_4 \psi_5 \rangle$	-0.1797893730	-0.1797893730	0
$\langle \psi_4 \psi_6 \rangle$	-0.1797893730	-0.1797893730	0
$\langle \psi_5 \psi_5 \rangle$	0.4562019590	0.4562019590	0
$\langle \psi_5 \psi_6 \rangle$	-0.0697819075	0.0697819075	1.4×10^{-1}
$\langle \psi_6 \psi_6 \rangle$	0.4562019590	0.4562019590	0

Appendix D: Matrix elements of Hamiltonian and overlap of the determinants of several H_4 geometries

Here we present all matrix elements of the Hamiltonian and overlap of the determinants for H_4 geometries used to obtain the CC weights presented in the Section V.

TABLE IX: Hamiltonian matrix elements (in Hartree) between nonorthogonal SCGVb Slater determinants. Columns show the quantum-estimated matrix elements (PGHE quantum circuit), the classical Löwdin reference, and the absolute deviation $|\Delta H_{ij}|$. The target system is a rectangular H_4 molecule (0.7414×0.92675 Å). Only unique elements ($i \leq j$) are reported since the Hamiltonian matrix is Hermitian.

H_{ij}	Quantum Circuit	Löwdin reference	$ \Delta H_{ij} $
$\langle \psi_1 H \psi_1 \rangle$	-1.6035884013	-1.6296920868	0.0261036855
$\langle \psi_1 H \psi_2 \rangle$	0.1861899770	0.1922546039	0.0060646269
$\langle \psi_1 H \psi_3 \rangle$	0.2024651090	0.1922546039	0.0102105051
$\langle \psi_1 H \psi_4 \rangle$	-0.0503718171	-0.0500258244	0.0003459927
$\langle \psi_1 H \psi_5 \rangle$	0.5200942739	0.5202726591	0.0001783852
$\langle \psi_1 H \psi_6 \rangle$	0.5296038729	0.5202726591	0.0093312138
$\langle \psi_2 H \psi_2 \rangle$	-0.5832003218	-0.5722451592	0.0109551626
$\langle \psi_2 H \psi_3 \rangle$	-0.0601484921	-0.0576903182	0.0024581739
$\langle \psi_2 H \psi_4 \rangle$	0.1857931916	0.1922546039	0.0064614123
$\langle \psi_2 H \psi_5 \rangle$	-0.0068580786	-0.0046185579	0.0022395207
$\langle \psi_2 H \psi_6 \rangle$	-0.0032248990	-0.0046185579	0.0013936589
$\langle \psi_3 H \psi_3 \rangle$	-0.5933468267	-0.5722451592	0.0211016675
$\langle \psi_3 H \psi_4 \rangle$	0.1858430859	0.1922546039	0.0064115180
$\langle \psi_3 H \psi_5 \rangle$	-0.0029459046	-0.0046185579	0.0016726533
$\langle \psi_3 H \psi_6 \rangle$	-0.0066381811	-0.0046185579	0.0020196232
$\langle \psi_4 H \psi_4 \rangle$	-1.5985847263	-1.6296920868	0.0311073605
$\langle \psi_4 H \psi_5 \rangle$	0.5249557894	0.5202726591	0.0046831303
$\langle \psi_4 H \psi_6 \rangle$	0.5252628050	0.5202726591	0.0049901459
$\langle \psi_5 H \psi_5 \rangle$	-1.0517394094	-1.0404865434	0.0112528660
$\langle \psi_5 H \psi_6 \rangle$	-0.2456620275	-0.2454850444	0.0001769831
$\langle \psi_6 H \psi_6 \rangle$	-1.0460970146	-1.0404865434	0.0056104712

TABLE X: Overlap matrix elements between the six SCGVb determinants for rectangular H_4 (0.7414×0.92675 Å). The column “QA (DOE)” lists the values obtained from the quantum circuit, while “Löwdin rules” contains the classical reference. Absolute discrepancies are $|\Delta S_{ij}| = |S_{ij}^{\text{QA}} - S_{ij}^{\text{ref}}|$. Only unique elements ($i \leq j$) are reported since the overlap matrix is symmetric.

S_{ij}	QA (DOE)	Löwdin rules	$ \Delta S_{ij} $
$\langle \psi_1 \psi_1 \rangle$	0.7140258214	0.7140258214	0
$\langle \psi_1 \psi_2 \rangle$	-0.0790672997	-0.0790672997	0
$\langle \psi_1 \psi_3 \rangle$	-0.0790672997	-0.0790672997	1.58×10^{-1}
$\langle \psi_1 \psi_4 \rangle$	0.0201509724	0.0201509724	0
$\langle \psi_1 \psi_5 \rangle$	-0.1990186006	-0.1990186006	0
$\langle \psi_1 \psi_6 \rangle$	-0.1990186006	-0.1990186006	0
$\langle \psi_2 \psi_2 \rangle$	0.3201019318	0.3201019318	0
$\langle \psi_2 \psi_3 \rangle$	0.0188432867	0.0188432867	0
$\langle \psi_2 \psi_4 \rangle$	-0.0790672997	-0.0790672997	0
$\langle \psi_2 \psi_5 \rangle$	-0.0014028130	-0.0014028130	0
$\langle \psi_2 \psi_6 \rangle$	-0.0014028130	-0.0014028130	0
$\langle \psi_3 \psi_3 \rangle$	0.3201019318	0.3201019318	0
$\langle \psi_3 \psi_4 \rangle$	0.0790672997	-0.0790672997	1.58×10^{-1}
$\langle \psi_3 \psi_5 \rangle$	-0.0014028130	-0.0014028130	2.81×10^{-3}
$\langle \psi_3 \psi_6 \rangle$	-0.0014028130	-0.0014028130	0
$\langle \psi_4 \psi_4 \rangle$	0.7140258214	0.7140258214	0
$\langle \psi_4 \psi_5 \rangle$	-0.1990186006	-0.1990186006	0
$\langle \psi_4 \psi_6 \rangle$	-0.1990186006	-0.1990186006	0
$\langle \psi_5 \psi_5 \rangle$	0.5008812352	0.5008812352	0
$\langle \psi_5 \psi_6 \rangle$	-0.0779665852	-0.0779665852	1.56×10^{-1}
$\langle \psi_6 \psi_6 \rangle$	0.5008812352	0.5008812352	0

TABLE XI: Hamiltonian matrix elements (in Hartree) between nonorthogonal SCGVB Slater determinants. Columns show the quantum-estimated matrix elements (PGHE quantum circuit), the classical Löwdin reference, and the absolute deviation $|\Delta H_{ij}|$. The target system is a rectangular H_4 molecule ($0.7414 \times 1.2 \text{ \AA}$). Only unique elements ($i \leq j$) are reported since the Hamiltonian matrix is Hermitian.

H_{ij}	Quantum Circuit	Löwdin reference	$ \Delta H_{ij} $
$\langle \psi_1 H \psi_1 \rangle$	-1.8464182798	-1.8640455684	0.0176272886
$\langle \psi_1 H \psi_2 \rangle$	0.0936360199	0.0869394156	0.0066966043
$\langle \psi_1 H \psi_3 \rangle$	0.0880244225	0.0869394156	0.0010850069
$\langle \psi_1 H \psi_4 \rangle$	-0.2430388722	-0.2437304082	0.0006915360
$\langle \psi_1 H \psi_5 \rangle$	0.7815945022	0.7817148523	0.0001203501
$\langle \psi_1 H \psi_6 \rangle$	0.7914416464	0.7817148523	0.0097267941
$\langle \psi_2 H \psi_2 \rangle$	-0.5357262078	-0.5268539625	0.0088722453
$\langle \psi_2 H \psi_3 \rangle$	-0.0124061816	-0.0123280523	0.0000781293
$\langle \psi_2 H \psi_4 \rangle$	0.0848025242	0.0869394156	0.0021368914
$\langle \psi_2 H \psi_5 \rangle$	-0.0048022157	-0.0025821286	0.0022200871
$\langle \psi_2 H \psi_6 \rangle$	-0.0024764124	-0.0025821286	0.0001057162
$\langle \psi_3 H \psi_3 \rangle$	-0.5502374058	-0.5268539625	0.0233834433
$\langle \psi_3 H \psi_4 \rangle$	0.0843623245	0.0869394156	0.0025770911
$\langle \psi_3 H \psi_5 \rangle$	-0.0012726857	-0.0025821286	0.0013094429
$\langle \psi_3 H \psi_6 \rangle$	-0.0050026172	-0.0025821286	0.0024204886
$\langle \psi_4 H \psi_4 \rangle$	-1.8455586554	-1.8640455684	0.0184869130
$\langle \psi_4 H \psi_5 \rangle$	0.7954009424	0.7817148523	0.0136860901
$\langle \psi_4 H \psi_6 \rangle$	0.7864479610	0.7817148523	0.0047331087
$\langle \psi_5 H \psi_5 \rangle$	-1.5580916078	-1.5506245415	0.0074670663
$\langle \psi_5 H \psi_6 \rangle$	-0.3809163008	-0.3781083466	0.0028079542
$\langle \psi_6 H \psi_6 \rangle$	-1.5593865408	-1.5506245415	0.0087619993

TABLE XII: Overlap matrix elements between the six SCGVB determinants for rectangular H_4 ($0.7414 \times 1.2 \text{ \AA}$). The column “QA (DOE)” lists the values obtained from the quantum circuit, while “Löwdin rules” contains the classical reference. Absolute discrepancies are $|\Delta S_{ij}| = |S_{ij}^{\text{QA}} - S_{ij}^{\text{ref}}|$. Only unique elements ($i \leq j$) are reported since the overlap matrix is symmetric.

S_{ij}	QA (DOE)	Löwdin rules	$ \Delta S_{ij} $
$\langle \psi_1 \psi_1 \rangle$	0.8373995335	0.8373995335	0
$\langle \psi_1 \psi_2 \rangle$	-0.0380339632	-0.0380339632	0
$\langle \psi_1 \psi_3 \rangle$	0.0380339632	-0.0380339632	7.61×10^{-2}
$\langle \psi_1 \psi_4 \rangle$	0.0809005960	0.0809005960	0
$\langle \psi_1 \psi_5 \rangle$	-0.2983148141	-0.2983148141	0
$\langle \psi_1 \psi_6 \rangle$	-0.2983148141	-0.2983148141	0
$\langle \psi_2 \psi_2 \rangle$	0.3201019318	0.3201019318	0
$\langle \psi_2 \psi_3 \rangle$	0.0042106542	0.0042106542	0
$\langle \psi_2 \psi_4 \rangle$	-0.0380339632	-0.0380339632	0
$\langle \psi_2 \psi_5 \rangle$	-0.0013210424	-0.0013210424	0
$\langle \psi_2 \psi_6 \rangle$	-0.0013210424	-0.0013210424	0
$\langle \psi_3 \psi_3 \rangle$	0.3201019318	0.3201019318	0
$\langle \psi_3 \psi_4 \rangle$	0.0380339632	-0.0380339632	7.61×10^{-2}
$\langle \psi_3 \psi_5 \rangle$	-0.0013210424	-0.0013210424	0
$\langle \psi_3 \psi_6 \rangle$	-0.0013210424	-0.0013210424	0
$\langle \psi_4 \psi_4 \rangle$	0.8373995335	0.8373995335	0
$\langle \psi_4 \psi_5 \rangle$	-0.2983148141	-0.2983148141	0
$\langle \psi_4 \psi_6 \rangle$	-0.2983148141	-0.2983148141	0
$\langle \psi_5 \psi_5 \rangle$	0.7228499269	0.7228499269	0
$\langle \psi_5 \psi_6 \rangle$	-0.1220243610	0.1220243610	2.44×10^{-1}
$\langle \psi_6 \psi_6 \rangle$	0.7228499269	0.7228499269	0

TABLE XIII: Hamiltonian matrix elements (in Hartree) between nonorthogonal SCGVB Slater determinants. Columns show the quantum-estimated matrix elements (PGHE quantum circuit), the classical Löwdin reference, and the absolute deviation $|\Delta H_{ij}|$. The target system is a rectangular H_4 molecule ($0.7414 \times 1.26 \text{ \AA}$). Only unique elements ($i \leq j$) are reported since the Hamiltonian matrix is Hermitian.

H_{ij}	Quantum Circuit	Löwdin reference	$ \Delta H_{ij} $
$\langle \psi_1 H \psi_1 \rangle$	-1.8942763210	-1.9057425327	0.0114662117
$\langle \psi_1 H \psi_2 \rangle$	0.0709018507	0.0725345274	0.0016326767
$\langle \psi_1 H \psi_3 \rangle$	0.0771095406	0.0725345274	0.0045750132
$\langle \psi_1 H \psi_4 \rangle$	-0.2844217969	-0.2840928654	0.0003289315
$\langle \psi_1 H \psi_5 \rangle$	0.8311658625	0.8278481529	0.0033177096
$\langle \psi_1 H \psi_6 \rangle$	0.8342336179	0.8278481529	0.0063854650
$\langle \psi_2 H \psi_2 \rangle$	-0.5289858414	-0.5211398372	0.0078460042
$\langle \psi_2 H \psi_3 \rangle$	-0.0091121107	-0.0086104169	0.0005016938
$\langle \psi_2 H \psi_4 \rangle$	0.0693655891	0.0725345274	0.0031689383
$\langle \psi_2 H \psi_5 \rangle$	-0.0031278476	-0.0021944191	0.0009334285
$\langle \psi_2 H \psi_6 \rangle$	-0.0028232805	-0.0021944191	0.0006288614
$\langle \psi_3 H \psi_3 \rangle$	-0.5450522159	-0.5211398372	0.0239123787
$\langle \psi_3 H \psi_4 \rangle$	0.0698525691	0.0725345274	0.0026819583
$\langle \psi_3 H \psi_5 \rangle$	-0.0014004555	-0.0021944191	0.0007939636
$\langle \psi_3 H \psi_6 \rangle$	-0.0009935743	-0.0021944191	0.0012008448
$\langle \psi_4 H \psi_4 \rangle$	-1.8783532902	-1.9057425327	0.0273892425
$\langle \psi_4 H \psi_5 \rangle$	0.8387496303	0.8278481529	0.0109014774
$\langle \psi_4 H \psi_6 \rangle$	0.8363918543	0.8278481529	0.0085437014
$\langle \psi_5 H \psi_5 \rangle$	-1.6470579099	-1.6381039770	0.0089539329
$\langle \psi_5 H \psi_6 \rangle$	-0.3984998909	-0.4022735280	0.0037736371
$\langle \psi_6 H \psi_6 \rangle$	-1.6519666078	-1.6381039770	0.0138626308

TABLE XIV: Overlap matrix elements between the six SCGVB determinants for rectangular H_4 ($0.71414 \times 1.26 \text{ \AA}$). The column “QA (DOE)” lists the values obtained from the quantum circuit, while “Löwdin rules” contains the classical reference. Absolute discrepancies are $|\Delta S_{ij}| = |S_{ij}^{\text{QA}} - S_{ij}^{\text{ref}}|$. Only unique elements ($i \leq j$) are reported since the overlap matrix is symmetric.

S_{ij}	QA (DOE)	Löwdin rules	$ \Delta S_{ij} $
$\langle \psi_1 \psi_1 \rangle$	0.8584263458	0.8584263458	0
$\langle \psi_1 \psi_2 \rangle$	-0.0320637598	-0.0320637598	0
$\langle \psi_1 \psi_3 \rangle$	0.0320637598	-0.0320637598	6.41×10^{-2}
$\langle \psi_1 \psi_4 \rangle$	0.0938058736	0.0938058736	0
$\langle \psi_1 \psi_5 \rangle$	-0.3158337956	-0.3158337956	0
$\langle \psi_1 \psi_6 \rangle$	-0.3158337956	-0.3158337956	0
$\langle \psi_2 \psi_2 \rangle$	0.3201019318	0.3201019318	0
$\langle \psi_2 \psi_3 \rangle$	0.0029658965	0.0029658965	0
$\langle \psi_2 \psi_4 \rangle$	-0.0320637598	-0.0320637598	0
$\langle \psi_2 \psi_5 \rangle$	-0.0012516001	-0.0012516001	0
$\langle \psi_2 \psi_6 \rangle$	-0.0012516001	-0.0012516001	0
$\langle \psi_3 \psi_3 \rangle$	0.3201019318	0.3201019318	0
$\langle \psi_3 \psi_4 \rangle$	0.0320637598	-0.0320637598	6.41×10^{-2}
$\langle \psi_3 \psi_5 \rangle$	0.0012516001	-0.0012516001	2.50×10^{-3}
$\langle \psi_3 \psi_6 \rangle$	-0.0012516001	-0.0012516001	0
$\langle \psi_4 \psi_4 \rangle$	0.8584263458	0.8584263458	0
$\langle \psi_4 \psi_5 \rangle$	-0.3158337956	-0.3158337956	0
$\langle \psi_4 \psi_6 \rangle$	-0.3158337956	-0.3158337956	0
$\langle \psi_5 \psi_5 \rangle$	0.7604763634	0.7604763633	1.0×10^{-10}
$\langle \psi_5 \psi_6 \rangle$	-0.1301315366	0.1301315367	2.60×10^{-1}
$\langle \psi_6 \psi_6 \rangle$	0.7604763634	0.7604763633	1.0×10^{-10}